Dalton Transactions

ROYAL SOCIETY OF CHEMISTRY

PERSPECTIVE

View Article Online
View Journal | View Issue

Cite this: *Dalton Trans.*, 2024, **53**, 14551

Recent advances and perspectives for intercalation layered compounds. Part 2: applications in the field of catalysis, environment and health

Chiara Bisio, *[a,b] Jocelyne Brendlé, *[c] Sébastien Cahen, [d] Yongjun Feng, [e] Seong-Ju Hwang, [f] Morena Nocchetti, *[g] Dermot O'Hare, [h] Pierre Rabu, [i] Klara Melanova [j] and Fabrice Leroux *[k]

Received 13th March 2024,
Accepted 17th June 2024

DOI: 10.1039/d4dt00757c

rsc.li/dalton

Intercalation compounds represent a unique class of materials that can be anisotropic (1D and 2D-based topology) or isotropic (3D) through their guest/host superlattice repetitive organisation. Intercalation refers to the reversible introduction of guest species with variable natures into a crystalline host lattice. Different host lattice structures have been used for the preparation of intercalation compounds, and many examples are produced by exploiting the flexibility and the ability of 2D-based hosts to accommodate different guest species, ranging from ions to complex molecules. This reaction is then carried out to allow systematic control and fine tuning of the final properties of the derived compounds, thus allowing them to be used for various applications. This review mainly focuses on the recent applications of intercalation layered compounds (ILCs) based on layered clays, zirconium phosphates, layered double hydroxides and graphene as heterogeneous catalysts, for environmental and health purposes, aiming at collecting and discussing how intercalation processes can be exploited for the selected applications.

1. Introduction

Intercalation is a way to specifically tune the structure, composition, and physico-chemical properties of materials by exploiting interactions between a host matrix (generally a 2D-layered material) and guest species of various chemical natures. Intercalation materials thus represent a broad class of compounds generated by the reversible insertion of guest species, which can range from ions to organic species, into a layered host matrix that can have either an amorphous or crystalline structure. As a result of the intercalation procedure, the structure of the host normally remains unmodified, or it is only slightly modified in the guest–host complex. The intercalation reaction can be chemically or thermally reversible, and it can be carried out using different approaches including insertion and introduction or topotactic exchange of atomic or molecular species inside the host matrix, thus allowing a controlled and systematic tuning of the physico-chemical properties.

As a general feature, intercalation layered compounds (ILCs) prepared by the different methods described in the first part of this perspective paper are a class of very flexible compounds because the appropriate choice of host and guest species results in the possibility of tuning their final properties, thus spreading their potential application to numerous technological fields.

These materials can be suitable for many applications, for instance as catalysts, sorbents, electrochromic displays, elec-

[a]*Dipartimento di Scienze e Innovazione Tecnologica, Università del Piemonte Orientale, Viale Teresa Michel 11, 15121 Alessandria, AL, Italy. E-mail: chiara.bisio@uniupo.it*
[b]*CNR-SCITEC Istituto di Scienze e Tecnologie Chimiche "Giulio Natta", Via C. Golgi 19, 20133 Milano, MI, Italy*
[c]*Institut de Science des Matériaux de Mulhouse CNRS UMR 7361, Université de Haute-Alsace, Université de Strasbourg, 3b rue Alfred Werner, 68093 Mulhouse CEDEX, France. E-mail: jocelyne.brendle@uha.fr*
[d]*Institut Jean Lamour – UMR 7198 CNRS-Université de Lorraine, Groupe Matériaux Carbonés, Campus ARTEM – 2 Allée André Guinier, B.P. 50840, F54011, NancyCedex, France*
[e]*State Key Laboratory of Chemical Resource Engineering, Beijing Engineering Center for Hierarchical Catalysts, Beijing University of Chemical Technology, No. 15 Beisanhuan East Road, Beijing, 100029, China*
[f]*Department of Materials Science and Engineering, College of Engineering, Yonsei University, Seoul 03722, Republic of Korea*
[g]*Department of Pharmaceutical Sciences, University of Perugia, Via del Liceo 1, 06123 Perugia, Italy. E-mail: morena.nocchetti@unipg.it*
[h]*Chemistry Research Laboratory, University of Oxford Department of Chemistry, 12 Mansfield Road, Oxford, OX1 3TA, UK*
[i]*Institut de Physique et Chimie des Matériaux de Strasbourg, CNRS – Université de Strasbourg, UMR7504, 23 rue du Loess, BP43, 67034 Strasbourg cedex 2, France*
[j]*Center of Materials and Nanotechnologies, Faculty of Chemical Technology, University of Pardubice, Studentská 95, 532 10 Pardubice, Czech Republic. E-mail: klara.melanova@upce.cz*
[k]*Institut de Chimie de Clermont-Ferrand, Université Clermont Auvergne, UMR CNRS 6296, Clermont Auvergne INP, 24 av Blaise Pascal, BP 80026, 63171 Aubière cedex, France. E-mail: fabrice.leroux@uca.fr*

trodes for secondary batteries (Li-ion batteries), components for fuel cells and drug delivery systems. The different intercalation approaches can be indeed used for: (i) modifying the catalytic, optic, electronic and magnetic performances of different host structures through the introduction of specific functionalities; (ii) thermally stabilising and protecting the guest species from light and oxygen; (iii) developing multifunctional carriers for specific applications.

In this review, representative examples from the state of the art of the last 8 years (since 2015) of the application of intercalation materials in the fields of catalysis, environment, health and polymeric composites are reported.

This perspective is especially focused on selected cationic and anionic layered materials as host matrices for the preparation of intercalation compounds.

Emphasis is placed on the use cationic layered materials such as clays, of both natural and synthetic origin (Fig. 1), and zirconium phosphates (ZrP). Layered double hydroxides (LDHs) are considered for the class of anionic layered materials (Fig. 2). Some recent examples of ILCs derived from graphene are also reported.

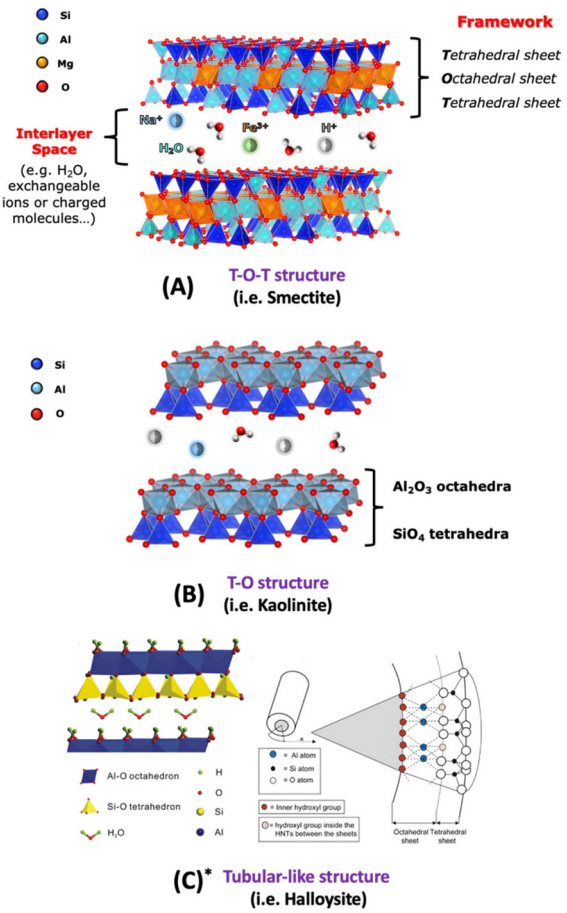

Fig. 1 Schematic view of different clay structures: T-O-T (A), T-O (B) structures and tubular-like structure (C* is adapted with permission from ref. 1, Copyright 2020 MDPI).

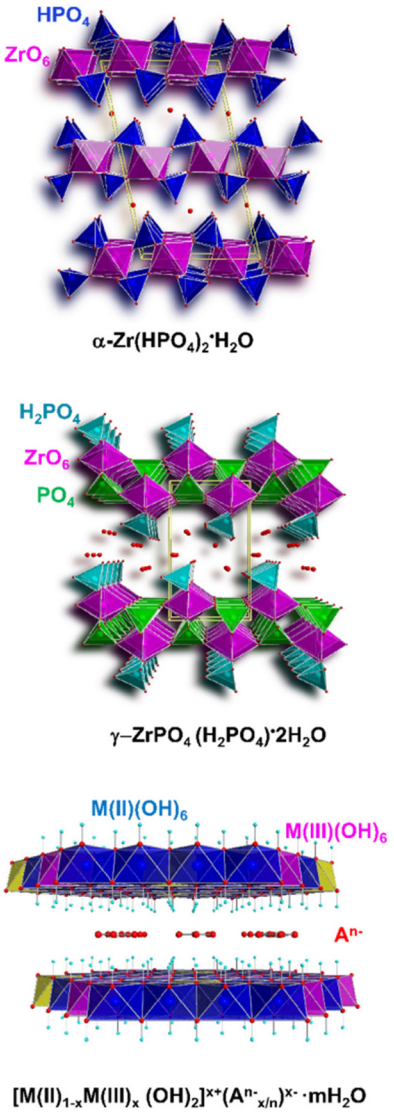

Fig. 2 Schematic view of α-ZrP, γ-ZrP and LDHs structures.

The number of scientific manuscripts reporting solids based on clays, ZrP, LDH for the applications of interest (*e.g.* heterogeneous catalysis, environment and health) in the last decade deserves great attention. The amount of papers dealing with the use of selected matrices for the different applications is reported in the histograms of Fig. 3.

In the following sections, the contributions of the selected solids in the different applications are reported, with the focus of attention on ILCs prepared by using clays, ZrP, LDHs and graphene.

1.1 Catalytic applications of intercalation compounds

In this section particular emphasis will be placed on the description of recent applications of intercalation compounds based on clays, ZrP and LDHs for heterogeneous catalysis.

1.1.1 Clay-based catalysts. Modified cationic clays (*e.g.* acid-treated clays) have been used in oil cracking reactions

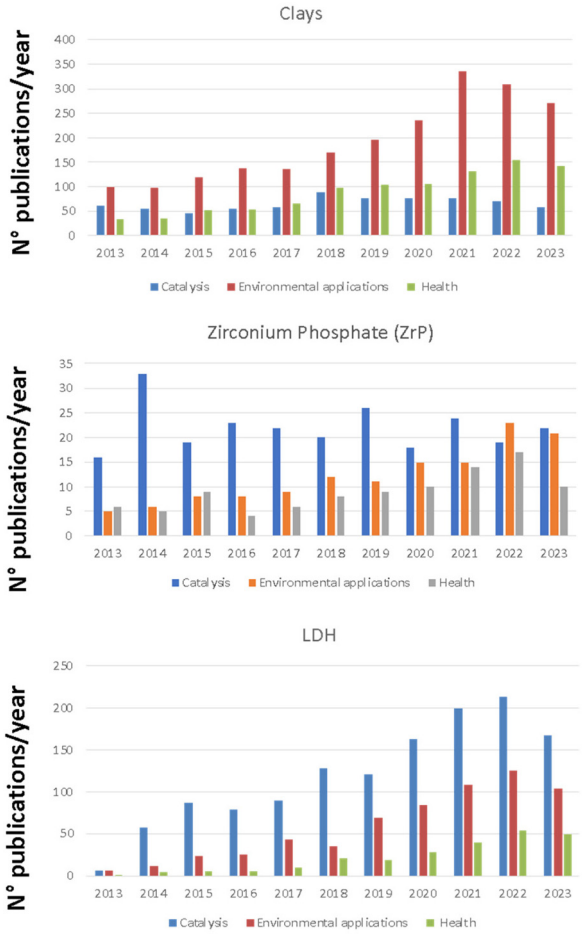

Fig. 3 Histograms reporting the amount of publications/year for clays, LDHs and ZrP for the selected applications. Data are obtained from SCOPUS database.

since the 1930s. Their use for catalytic purposes has been partially substituted by zeolites and porous materials since the 1960s. However, modification processes such as acid activation, ion exchange, pillaring procedures, preparation of composites and hybrids or hierarchical structuring of clays allowed the preparation of different families of intercalation compounds, proposed as heterogeneous catalysts.[1,2]

Clay-based catalysts have been used in the conversion of crude oil to biodiesel, and they are employed as catalysts for several reactions such as esterification, addition, transesterification, oxidation, hydrogenation, epoxidation, alkylation, polymerisation, allylation, diazotisation, acylation, rearrangement, isomerisation, cyclisation condensation, organic synthesis *etc*.[3,4] It was pointed out that catalysts derived from layered silicate are regenerable, low cost, and active not only for producing biodiesel but also for other chemical processes such as oxidation reactions, water treatment and photovoltaic applications. These solids showed efficient catalytic potential, allowing a high yield of FAMEs (fatty acid methyl esters) at less harsh reaction conditions, and they were proved to be easily recoverable, highly reusable and thus highly sustainable.[2]

Among clays, halloysite nanotube (HNT)-based heterogeneous catalysts deserve additional comments. Composite and hybrid materials obtained by the surface modification of halloysite, a natural clay with tubular morphology, are much proposed in the literature. It was observed that the synergy between halloysite and different modifying species (*i.e.* polymers, dendrimers, porphyrin, metal organic frameworks (MOFs), ionic liquids) allows an increase in the performance of the final hybrid/composite. However, the use of halloysite-based hybrids/composites also has some disadvantages due to the time-consuming multistep production processes, often involving (toxic) solvents/reagents for the large-scale production of these materials.[5] Modified halloysites have been also proposed for environmental and catalytic applications. For this latter application, the presence of metal nanoparticles (NPs) is essential to impart catalytic performance. Besides methods allowing the introduction of NPs on the outer surface of halloysite, the methods to embed metallic NPs of small size in the inner part of HNTs have been recently reviewed.[6] These methods have the advantage of increasing the resistance of NPs to cleavage and agglomeration of the embedded metallic NPs, thus improving the catalytic activity of the obtained solid.

Jiang *et al.* prepared Pd/HNTs by exploiting a modification of the hydrophobicity of halloysite by impregnating the solid with CTAB species (see Fig. 4). The proposed method allowed the authors to obtain uniformly dispersed palladium particles (*ca.* 2 nm), with a suitable ratio of Pd^{2+}/Pd^{4+} species and appropriate surface acidity: this solid showed improved catalytic activity with respect to the catalyst prepared without adding CTAB.[7]

For methane combustion, high-performance halloysite-supported palladium catalysts have been also proposed through appropriate pre-treatments of the support.[8]

Cu–Ni-containing halloysite solids prepared by ligand-assisted reduction of Cu^{2+} and Ni^{2+} cations followed by annealing have been also tested for the purification of vehicle exhaust gases through catalysed processes.[9] For this process, catalysts based on confinement of Cu–Ni species, Pd, and Ag (particle size below 3 nm) have been proposed. It was shown that the nano-confinement allows an increase in the stability

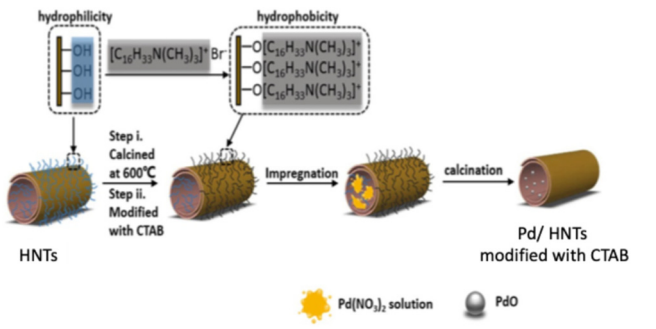

Fig. 4 Schematic diagram of the preparation method of Pd/HNTs catalyst. Adapted with permission from ref. 7, Copyright 2020, American Chemical Society.

of embedded NPs, reducing detachment and sintering, and improving the catalytic reaction kinetics.[6]

Modification of the clay's chemical composition was also proposed to introduce catalytic active sites into the clay framework, thus leading to active materials for the catalytic decomposition and/or simultaneous detection of toxic molecules, *e.g.* chemical warfare agents.[10–12] In this case, the synergistic presence of proton sites (normally introduced by ion exchange in acidic aqueous solutions) and metal centres (either present naturally in clays or introduced by modifying the preparation steps of the support) are beneficial for the catalytic performances of the final material.

Thermally stable pillared clays (or pillared interlayered clays, PILCs) derive from the intercalation of inorganic polycations in the clay interlayer space. The clay pillaring procedure allowed the preparation of solids mainly based on transition metal species, with great interest in the catalytic purposes particularly required in advanced oxidation processes and chemical transformations. The pillaring procedure allows the introduction of specific catalytic species on the clay's surface and this, together with the improvement in specific surface area and thermal stability, makes these solids suitable for different catalytic reactions (*e.g.* nitration of chlorobenzene, catalytic combustion of acetone, methyl-ethyl-ketone), oxidation and isomerisation reactions and as Fenton-like systems for the degradation of organic pollutants in wastewaters.[13] Clays pillared with TiO_2 (Ti-PILC) are characterised by surface acidity higher than other pillared clays, such as Al or Zn-PILC.[13] The origins of Brønsted and Lewis acid sites in Ti-PILC have been studied.[14] The photocatalytic degradation of organic species (*i.e.* organic dyes, herbicides and aromatic amines, phenolic compounds, emerging contaminants) over PILCs with TiO_2 species has been recently reviewed, with particular emphasis on photocatalysts based on kaolinite, palygorskite, montmorillonite and halloysite.[15]

Very recently, the use of PILCs for the catalytic reduction of NOx with hydrocarbons at low temperature was reviewed.[16] Special interest was paid to metal-supported PILCs, and the catalytic performances of different samples together with the possible reaction mechanisms in relation to the different active sites, metal loading and reaction conditions were reported. It was underlined that Ag- and Cu-based PILC displayed good performances for NOx conversion in the presence of short hydrocarbons (HC) at low temperature. Nevertheless, additional studies are needed to better clarify the HC-SCR reaction mechanisms in the presence of metal-modified PILC catalysts. Major challenges are represented by the preparation of stable metal-modified PILC catalysts for NOx reduction in the presence of H_2O and SO_2.[16]

Moreover, TiO_2/clay heterostructures for the remediation of water polluted by organic species have been recently proposed.[17] In this respect, particular emphasis was placed on the use of phyllosilicates as supports (*e.g.* montmorillonite, sepiolite, palygorskite, vermiculite, saponite). The introduction of pillars in the clays' galleries results in a stable porosity leading to heterostructured materials with high specific surface area (SSA) characterised by the presence of micro- and mesopores. The pore architecture and the high SSA have a positive effect on the photocatalytic activity of TiO_2/clay materials. Moreover, long-chain hydrophobic cationic surfactants can be exploited to tune the porosity of TiO_2-based clays and to produce porous clay heterostructures (PCHs) and delaminated porous clay heterostructures (DCPHs).[18–20]

These composite materials have been proposed for overcoming the problems related to practical and environmental issues linked to the use of nanosized TiO_2 powders. Different clays such as kaolinite, hectorite, saponite, montmorillonite, palygorskite, halloysite and imogolite have been proposed as support materials for TiO_2 nanoparticles, thus obtaining solids with high photocatalytic efficiency and easy separation from treated water. The different examples reported in the literature suggested that the combination of clay support characterised by high specific surface areas and adsorption capacity improves the photocatalytic activity of TiO_2 nanoparticles and thus the decomposition capacity for organic pollutants. It was pointed out that the anchoring of TiO_2 on the clay's surface is useful to reduce the TiO_2 agglomeration, thus leading to more active surface sites.[15]

A schematic representation of the formation of PILC and PCH starting from intercalation processes is reported in Fig. 5.

1.2 Catalytic applications of zirconium phosphate (ZrP)

ZrP can be also considered as a promising material for catalytic applications. ZrP shows very interesting physical and chemical properties, such as high ion-exchange capacity, good chemical and thermal stability, and easy functionalisation. The presence of acidic P-OH groups on the layers makes this solid an efficient catalyst in acid-catalyzed reactions. The acidity and the hydrophobicity of the ZrP surface can be modulated by totally or partially replacing the phosphate groups with other phosphonate groups. The modification of the ZrP surface has also been achieved by exploiting the reactivity of the surface hydroxyl groups with organofunctional silanes that allowed the immobilisation of catalytically active

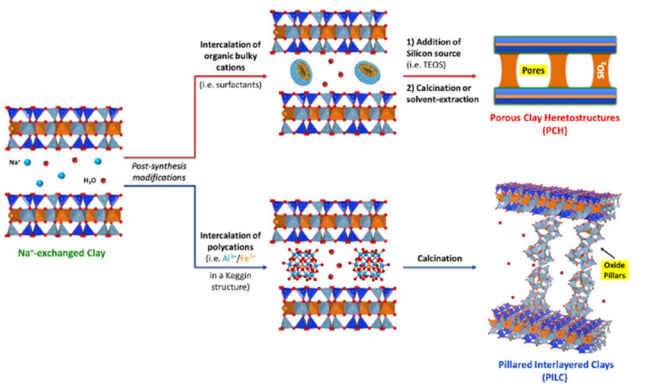

Fig. 5 Schematic view of the intercalation processes leading to the formation of porous clay heterostructures (PCH) and pillared interlayer clays (PILC).

nanoparticles.[21,22] Moreover, several catalysts have been prepared considering the ion-exchange capacity of ZrP. Intercalation compounds containing metal ions or metal complexes have shown good performance as catalysts for converting biomass-derived molecules into added-value products such as oxygenated fuels and fine chemicals. In particular, ZrP-Ru(III) and Ni/ZrP (Fig. 6A) showed high catalytic activity towards the oxidation of 5-hydroxymethylfurfural (HMF) under mild conditions.[23,24] ZrP intercalated with Ru(II) complex ([(*p*-cymene)Ru(phen)Cl]Cl) showed higher catalytic performance in selective hydrogenation, with molecular H_2, of the C=O group of furfural and of other carbonyl compounds into the corresponding alcohols. Experimental study and DFT calculation gave evidence that the catalytic performance can be attributed to the interaction of –POH groups of ZrP and Ru complex, leading to Ru–O–P active species.[25] Cu/ZrP catalyst enabled the direct oxidation of phenol, also derived from lignin depolymerisation, to *cis*,*cis*-muconic acid that can be further converted into high-added-value chemicals.[26]

Composite ZrP/silver-based materials are obtained by exploiting the intercalation properties of ZrP and then used as catalysts for the degradation of organic pollutants. Silver-exchanged ZrP treated with halogenidric acids gave rise to ZrP/AgX (X = Cl and Br) composites able to catalyze the photodegradation of rhodamine B (RhB). The action of ZrP as a source of silver ions led to a reduction of AgCl particle growth and aggregation, thus increasing the number of catalytic active sites. In addition, the –POH groups of ZrP promote the chemisorption of the RhB and then its degradation.[27,28] A composite ZrP-polydopamine (ZrP@PDA) was prepared by polymerization of dopamine in the aqueous dispersion of exfoliated ZrP. The catechol groups of PDA reduced the noble metal ions, such as silver or gold, generating metallic NPs on the ZrP@PDA surface. These composites showed very interesting catalytic activity towards the reduction of 4-nitrophenol to 4-aminophenol (Fig. 6B).[29,30] The exfoliation/restacking method was exploited to immobilise Pd precursor ($Pd(NH_3)_4Cl_2$) on α-ZrP nanosheets. The treatment with a reducing agent gave rise to Pd NPs, with an average diameter of 5.17 nm, immobilised on ZrP nanosheets (Fig. 6C). The composite showed good performance as a heterogeneous catalyst for the Heck reaction.[31]

Due to ZrP's electrochemical inertness it has been studied as a support for transition metals for the electrocatalysis of the oxygen evolution reaction (OER) in alkaline media.[32] Ions Fe^{2+}, Fe^{3+}, Co^{2+}, and Ni^{2+} were intercalated or adsorbed on α-ZrP material. The systems display interesting activity for the OER, requiring between 0.5–0.7 V of overpotential to reach 10 mA cm^{-2} (the benchmark for OER catalyst activity). It was found that the OER occurs especially on the external surfaces of the nanoparticles, thus the catalytic activity increases upon the exfoliation of ZrP materials.[33] Moreover, the OER activity depends on the loading and coverage of cobalt and nickel on ZrPs with different morphologies.[34] More recently, mixtures of nickel–iron were confined in ZrP; the hydrated confined environment of the layered structure stabilised Fe-rich compositions, yielding highly active OER catalysts.[35]

Carbon-free electrocatalysts for the oxygen reduction reaction in polymer electrolyte membrane fuel cells were prepared by growing Pt nanoparticles on ZrP, which is a solid-state proton conductor (Fig. 6D). The Pt/ZrP composites showed high durability and superior performance with respect to commercially available platinum-supported carbon catalysts.[36]

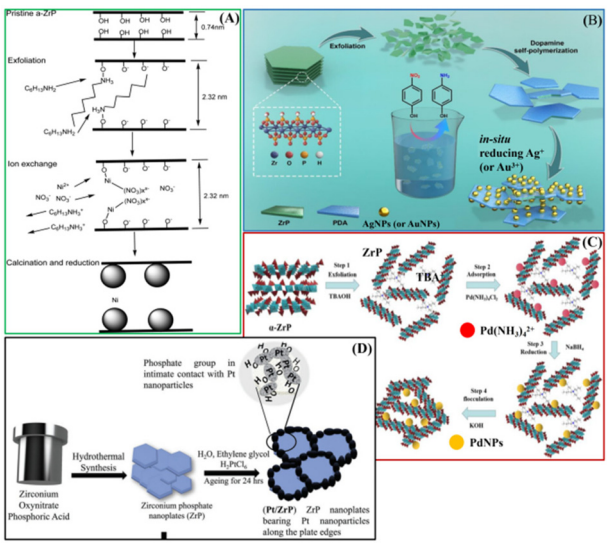

Fig. 6 Schematic illustration of preparation steps of the catalysts: (A) Ni/ZrP adapted with permission from ref. 24, Copyright 2018 American Chemical Society; (B) ZrP@PDA/AuNP or ZrP@PDA/AuNP, adapted with permission from ref. 30, Copyright 2020 MDPI; (C) ZrP-PdNPs, adapted with permission from ref. 31, Copyright 2022 Taiwan Institute of Chemical Engineers; (D) Pt/ZrP. Adapted with permission from ref. 36, Copyright 2023 John Wiley and sons.

1.3 Catalytic applications of LDHs

A recent review underlines the versatility of LDHs as anion-exchange frameworks as well as considering their ability to face today's societal issues, such as their high biocompatibility combined with their relatively low impact in terms of biodegradation.[37] LDHs are used in photocatalysis, electrocatalysis, CO_2 handling, biomass conversion, lowering the anthropogenic effects on the environment as scavenger for pollutants for water and soil treatments, and as additives for polymer and for polymer coatings.

The importance of the use of catalysts with reduced size (nano-catalysts) is covered in an interesting review focused on biomass conversion including reduction, oxidation or reforming reactions.[38] The tunability of the chemical composition of LDHs, associated with the flexibility to accommodate interleaved guests and a developed surface that can provide exposed and well-dispersed active species (for example metals or nanoparticles in an atomic-level uniform distribution) make LDH-based materials suitable and efficient nano-catalysts.

This is exemplified by de(hydrogenative) transformations and catalytic hydrogenations using transition metals in LDHs,[39] and more specifically Ni-based LDH to catalytically convert bio-ethanol to butanol.[40] In the latter case, the aldol-

condensation to use biomass and produce butanol was optimised from a supported Cu/NiAlOx material in a time-on-stream of 110 h at 280 °C reaching appropriate performance in terms of ethanol conversion, butanol selectivity and catalyst stability. Adapted cation composition as well as particle size can stabilise LDHs even in an acidic medium. For instance, $LiAl_2$ LDH-based sheets prepared by a urea method were covered with NHC-heterocyclic carbene gold anionic complexes for a reaction of hydration of alkynes.[41] Another study reports LDH of Mg_4Al composition covered this time by silver NP for the alkylation of nitriles, oxindoles and other carboxylic acid derivatives with alcohols.[42] In this study NP and the LDH support are co-acting in the cyclisation of *N*[2-(hydroxymethyl) phenyl]-2-phenylacetamides to yield 3-arylquinolin-2(1H): NP in the dehydrogenation and hydrogenation steps, while the LDH support catalyses the condensation step.

LDHs are also studied as photocatalysts; a recent review covers the latest advances in that domain[43] as well as electrocatalysts, mostly for the water-splitting to produce green hydrogen as well as other compound families such as transition metal chalcogenides.[44] As far as water electrolysis is concerned, they should possess electrocatalytic activity associated with long-term stability. LDHs rank well for developing such sustainable and clean energy, as discussed in critical reviews[45,46] where the relationships between structural defects and electrocatalytic performances are scrutinised, as for Ce-doped NiFe LDH-based material dispersed onto carbon paper[47] or NiFe heterostructure nanorods[48] for the OER. Other interesting articles mainly focus on LDHs and the possibility for seawater electrolysis, since they are stable in alkaline electrolyte suitable for seawater oxidation at the anode through the OER and not that of chloride ions.[49] However, NiFe LDHs-based electrocatalysts for the OER suffer from instability upon cycling, mostly due to the leaching of Fe active sites migrating out of the structure to form ferrihydrite by-product after repetitive potential cycling.[50]

Among 2D carbon-based materials, iron- and nitrogen-doped graphene appear as promising platinum-free materials for the oxygen reduction reaction (ORR),[51] and g-C_3N_4 and other doped graphenic materials (*i.e.* single or double doping with N, B, S and P) for ORR, hydrogen evolution (HER), and reports of OER rivalling that of noble metals and transition metal-based catalysts have been reviewed by Chen *et al.*[52]

The examples described above are summarised in Table 1. Wherever possible, the catalytic performances of ILCs are compared with those of reference materials (*e.g.* non-hybridised systems, non-intercalated heterogeneous catalysts).

2. Environmental applications of intercalation materials

This section is devoted to the description of the most representative examples of intercalation compounds based on clays, ZrP and LDHs for the removal of environmental contaminants. An overview of the most significant examples of these materials for environmental applications is also reported in Table 2.

2.1 Environmental applications of clays

Clay minerals have been largely studied in the last few decades as solid adsorbents to remove heavy metals with high toxicity (*i.e.* cadmium, copper, lead, zinc, chromium(VI) but also mercury, cobalt, manganese, chromium(III)), organic dyes and other pollutants (*i.e.* antibiotics, per- and polyfluoroalkyl substances, organic species...) from aqueous solutions and industrial wastewaters.[53–57] Natural clays are used because of their non-toxic nature, low cost, wide availability, and high adsorption capabilities. Examples of clay modifications to allow the detection of specific anions are also given.[58]

Natural clays are very often modified by using thermal treatments, acid washing, pillaring strategies, or through the intercalation of organic species in the galleries, aiming at improving adsorption properties. Materials such as clay nanosheets, nanotubes, nanorods and clay-supported nanoparticles are reported.[59] In this respect, interesting recent approaches are linked to clay exfoliation processes to obtain low-dimensional clays (with 1D or 2D morphology). This method is used to fully expose adsorption sites and to increase the specific surface area of the adsorbents.[60,61]

Moreover, coupling agents and/or polymers are used to create nano-clay-based composites with a porous structure allowing exploitation of the exposed adsorption sites and/or introduction of functional groups aiming at increasing the affinity to heavy metals and toxic dyes.[59]

Clays have been also proposed as supports for nanoparticles of metals and metal oxides (*i.e.* iron and copper oxides, TiO_2, ZnO, Al_2O_3), thus obtaining more effective adsorbing agents. As an example, the presence of Fe_3O_4 on halloysite nanotubes has been proposed for treating the excess of phosphate in water media: it was reported that the supported metal species improves the clay surface charge density thus leading better phosphate control.[62] The presence of the clay seems to improve the adsorption capacity of the pristine Fe_2O_3 species towards arsenite species.[63]

Supported metal oxide species are also useful for the degradation of toxic species. The case of nanoparticle-sized zero-valent iron (normally named nZVI or nFe0) deserves special attention in wastewater and groundwater remediation because of its ability in the degradation and removal of different metals (*i.e.* As, Cr(VI)), Pb and other toxic pollutants.[64–66]

The combination of nZVI and clay support is a positive strategy to avoid the aggregation of metal species, thus allowing the development of effective systems for water remediation. The use of these composite systems was systematically reviewed in 2017.[67]

The preparation and use of several types of clay-based composite materials for contaminant remediation (with emphasis on heavy metals, nitrate, selenate, dyes, nitroaromatic compounds, polybrominated diphenyl ethers and chlorinated compounds) are also reported. Data related to an extended use of the type of nanocomposites for the removal of chlorinated

Table 1 Most representative examples of intercalation compounds based on clays, ZrP and LDHs for the catalytic applications. Results described in the reviews are not reported

Catalyst	Active species	Catalyst preparation	Reaction	Substrate	Catalytic conditions	Products	Ref.
Pd/HTNs	Pd	CTAB surface modification, impregnation and calcination	Oxidation	Methane	0.2 g catalysts with 1 wt% Pd nominal loading; gas feed: 1 vol% CH_4, 10 vol% O_2 in N_2 Flow rate: 100 mL min^{-1} *T*: 425–620 °C	Methane conversion: 99% at 425 °C, *ca.* 195 °C lower than of Pd/HNTs prepared without any surface modification	7
Pd/HNTs	Pt	Surface modification using acid, basic media and surfactants, impregnation, calcination	Oxidation	Methane	50 mg catalysts $CH_4 : O_2 : Ar$ (1% : 20% : 79%) Flow rate: 60 mL min^{-1} *T*: 250–450 °C	Methane conversion depends on the surface treatment. Best performances with Pd/HNTs-NaOH that shows 90% conversion at 373 °C.	8
Cu-Ni/HTNs	Metallic Cu and Ni particles	Wet chemical synthesis	Rreduction	Simulated exhaust gas (equimolar mixture of nitrogen monoxide and carbon monoxide)	10 mg catalysts, NO (5.00 kPa) and CO (5.00 kPa) *T*: 275–400 °C	NO conversion to N_2: over 90% at 325 °C after 30 min.	9
Nb/saponite	Nb in framework position	Nb introduction in framework position	Selective oxidation	(2-Chloroethyl)ethylsulfide (CEES)	20 mg catalyst	CEES conversion: 98% (8 h)	10
Synthetic saponite clay	Intercalated H^+ species				14 mM CEES; 70 mm 30% aq. H_2O_2; *n*-heptane; *T*: 25 °C	Selectivity to CEESO: 73% Synthetic saponite clay (without Nb and protons): CEES conversion *ca.* 20% (8 h)	
Fe/montmorillonite	Fe^{3+} and H^+	Ion exchange of montmorillonite natural clay	Selective oxidation	(2-Chloroethyl)ethylsulfide (CEES)	20 mg catalyst	CEES conversion: >99% over acid sample after 48 h	11
H/montmorillonite Commercial (non modified) sample					14 mM CEES; 70 mm 30% aq. H_2O_2; *n*-heptane; *T*: 25 °C	The parent sample (without any modification): CEES conversion of 7.5% after 48 h	
TiO_2-MMT PLC	TiO_2	Intercalation of Ti alkoxide precursor with supercritical CO_2	Photocatalytic degradation	Toluene and acetaldehyde	Toluene (100 vol ppm) and acetaldehyde (500 vol ppm) in humidified air, 250 W high-pressure mercury lamp	VOCs decomposition rate between 2 and 6 mol min^{-1} mol^{-1} TiO_2	18
TiO_2-MMT PLC	TiO_2	Acidic solutions of hydrolyzed Ti alkoxides in the presence of high-molecular-weight polymer	Photocatalytic degradation	Methylene blue (MB)	Aqueous suspensions of MB (250 ml, initial concentration 30 mg l^{-1}) and photocatalyst powder (50 mg), 250 W high-pressure mercury lamp	Maximum removal efficiency of methylene blue is for PIL up to 83% within 90 min	19
Compared with TiO_2 P25						For P25: degradation efficiency *ca.* 46%	

Table 1 *(Contd.)*

Catalyst	Active species	Catalyst preparation	Reaction	Substrate	Catalytic conditions	Products	Ref.
Multicomponent PCHs	SiO_2/Al_2O_3, SiO_2/TiO_2 and Si/ZrO_2 pillars	Pillaring by surfactant directed methods and template ion exchange method.	Dehydration reactions	Methanol and ethanol	100 mg catalysts Gas mixture containing 3.9 vol% of methanol diluted in helium (total flow rate of 20 ml min^{-1}, isothermal saturator at 0 °C) or 5.7 vol% of ethanol diluted in pure helium (total flow rate of 20 ml min^{-1}, isothermal saturator at 20 °C) *T*: between 100 and 325 °C	Methanol conversion to dimethyl ether (DME): between 40 and 77% at 300 °C (best results obtained in the presence of SiO_2 pillars) Ethanol conversion to diethyl ether (DEE) and ethylene: between 80 and 100% at 300 °C (best results achieved in the presence of Al_2O_3 pillars)	20
ZrP-Ru	Ru(III)	Ion-exchange	Oxidation	5-Hydroxymethylfurfural	*T* = 110 °C *P* = atmospheric O_2 pressure, flow rate of 20 ml min^{-1} *t* = 12 h	2,5-Furandicarboxylic acid (selectivity: 28%) 2,5-Diformylfuran (selectivity: 62%)	23
Ni/ZrP	Ni, Lewis acidic sites of Zr(IV)	Exfoliation, ion-exchange, calcination and reduction	Hydrodeoxygenation	5-Hydroxymethylfurfural	*T* = 240 °C *P* = 5 MPa H_2 *t* = 20 h	2,5-Dimethylfuran (yield: 68.1%)	24
ZrP-[(*p*-cymene)Ru(phen)Cl] Compared with: Ru/C	Ru–O–P species formed by interaction of cationic Ru(II) complex and P-OH group of ZrP	Exfoliation, ion-exchange	Hydrogenation	Furfural	*T* = 100 °C *P* = 1.5 MPa H_2 *T* = 8 h	Furfuryl alcohol (selectivity: 99%) For Ru/C: furfuryl alcohol (selectivity: 34%)	25
Cu/ZrP Compared with: $Cu(OAc)_2$	Cu(II) bound with phosphate groups, Cu(II)–O–P species	Wet impregnation, calcination at 200 °C	Oxidation	Phenol	$HCOOH : H_2O_2 = 5 : 1$, 12 mmol H_2O_2, 0.2 mmol H_3PO_4 *T* = 30 °C *T* = 2 h	*cis*,*cis*-Muconic acid (selectivity: 60%; yield: 40%) For $Cu(OAc)_2$: *cis*,*cis*-muconic acid (selectivity: 55%; yield: 35%)	26
ZrP/AgCl Compared with: AgCl	Ag@AgCl	Ion-exchange, treatment with HCl	Photodegradation	Rhodamine B	mg AgCl per mL RhB = 0.74 $[RhB] = 10^{-5}$ M	Chromophore cleavage: 92% in 10 min For AgCl: chromophore cleavage: 57% in 30 min	27
ZrP/AgBr Compared with: AgCl	Ag@AgBr Ag@AgBr	Ion-exchange, treatment with HBr	Photodegradation	Rhodamine B	mg AgBr per mL RhB = 1.1 $[RhB] = 10^{-5}$ M	Chromophore cleavage: 90% in 3 min Chromophore cleavage: 91% in 30 min	28

Table 1 *(Contd.)*

Catalyst	Active species	Catalyst preparation	Reaction	Substrate	Catalytic conditions	Products	Ref.
ZrP@PDA/Ag Compared with: AgNPs/SNTs	AgNPs	Reduction and deposition of silver on ZrP-polydopamine	Reduction	4-Nitrophenol (4NP)	[4NP] = 0.12 mM, [$NaBH_4$] = 38 mM [Ag] = 0.125 μg mL^{-1} T = 25 °C	4-Aminophenol (apparent rate constant = 34.76 × 10^{-3} s^{-1}) For AgNPs/SNTs: 4-aminophenol (apparent rate constant = 38.41 × 10^{-3} s^{-1})	29
ZrP@PDA/Au Compared with: Au@MOF-3	AuNPs	Reduction and deposition of gold on ZrP-polydopamine	Reduction	4-Nitrophenol (4-NP)	[4NP] = 0.24 mM, [$NaBH_4$] = 76 mM [Ag] = 0.125 μg mL^{-1} T = 25 °C	4-Aminophenol (apparent rate constant = 7.4 × 10^{-3} s^{-1}) For Au@MOF-3: 4-aminophenol (apparent rate constant = 68.8 × 10^{-3} s^{-1})	30
Pd@ZrP Compared with: PS-TEA	PdNPs	Exfoliation, restacking, *in situ* reduction	Carbon–carbon bond formation	Iodobenzene (IB) and methyl acrylate (MA)	IB = 1.0 mmol, MA = 1.5 mmol NEt_3 = 1.5 mmol DMF = 2 mL, T = 100 °C, t = 0.5 h, Pd@ZrP = 15 mg, 0.204 mol% of Pd, NEt_3, GVL, 130 °C, 2 h	Methyl cinnamate (conversion: 95.8%) For PS-TEA: methyl cinnamate (conversion: 91%)	31
$Ni_{0.1}Fe_{0.9}$-ZrP Compared with: Ni1Fe2-250	Ni^{2+}/Fe^{3+}	Ion-exchange reaction	OER	Water	Catalyst loading = 0.125 mg cm^{-2} KOH = 0.1 M Catalyst loading = 0.17 mg cm^{-2}	Overpotential = 350 mV at 10 mA cm^{-2} For Ni1Fe2-250: overpotential = 310 mV at 10 mA cm^{-2}	35
Pt/ZrP Compared with: Pt/C	PtNPs	Ageing ZrP with H_2PtCl_6	Oxygen reduction reaction (ORR) in polymer electrolyte membrane fuel cells (PEMFC)	Oxygen	PEMFC at an operating potential of 0.60 V	Maximum power densities = 0.95 W cm^{-2} For Pt/C: maximum power densities = 0.83 W cm^{-2}	36
Cu/NiAl-LDH	Cu/NiAlOx	Hydrothermal deposition–precipitation method	Guerbet coupling reaction	Biomass-derived ethanol	T = 280 °C, P = 2 MPa N_2 T = 110 h	*n*-Butanol (conversion = 35%, selectivity = 25%)	40
LiAl2-LDH-NHC-Au(I)	Gold/carben complex NHC, Au(I)(NHC-Au(I))	Direct coprecipitation	Hydration	Alkynes alcohol (*i.e.* pent-4-ynol)	Catalyst = 0.75 mol% T = 60 °C t = 2 h pH = 3	5-Hydroxypentan2-one (conversion = 100%)	41
Ag/Mg_4Al-LDH	AgNPs and LDH		Formation of new C–C bonds from alcohols and C nucleophiles	Nitriles, oxindoles	Nitrile or oxindole = 0.125 mmol alcohol = 0.375 mmol Ag/Mg_4Al-LDH = 134 mg, 5 mol% Ag Mesitylene = 1.5 mL T = 140 °C under N_2 T = 24 h	Isolated products (yield = from 70% to 97%)	42

Table 1 *(Contd.)*

Catalyst	Active species	Catalyst preparation	Reaction	Substrate	Catalytic conditions	Products	Ref.
NiFeCe-LDH on carbon paper (CP) Compared with: commercial IrO_2 benchmark	Ni^{2+}/Fe^{3+}	Precipitation with urea	OER	Water	KOH = 1 M 50 μL of the ink (IrO_2 = 3 mg, nafion = 15 μL, ethanol = 1 mL) was dropped on CP KOH = 1 M	Overpotential = 232 mV at 10 mA cm^{-2} For IrO_2: overpotential = 451 mV at 10 mA cm^{-2}	47
NiFe-LDH/Fe1–N–C heterostructure hollow nanorods Compared with: Pt/C||IrO_2	NiFe-LDH and Fe1–N–C	Preparation of Fe1–N–C hollow nanorods through a ZIF-phase-transition principle, decoration with NiFe-LDH nanodots	Bifunctional ORR/OER in rechargeable Zn–air batteries	O_2/water	Catalyst (carbon cloth) as the air cathode, a zinc plate as the anode, 6 M KOH solution containing 0.2 M $Zn(Ac)_2$ filled between the electrodes as electrolyte.	Power density = 205 mW cm^{-2} ultralong cyclability up to 400 h For Pt/C||IrO_2: power density = 111.6 mW cm^{-2}	48

volatile organic compounds from soils are also discussed, and it was shown that concentration of pollutant species is strongly reduced.[68] Nevertheless, further studies to clarify the mechanism of degradation of various contaminants on nZVI/clay composites (*i.e.* adsorption, oxidation, reduction and precipitation processes) are still needed to optimise the preparation and application conditions of these materials.

Intercalation of natural clays with surfactants (*i.e.* quaternary ammonium cations (QACs)) aiming at improving the adsorption capacity for water pollutants has been also reviewed.[69] Introduction of QACs allows modification of the hydrophobicity of the clay surface and expansion of the interlayer space of 2D materials. Different types of surfactants have been already proposed for this use (*i.e.* organic surfactants with benzyl, phenyl, tetramethylammonium (TMA), trimethylphenylammonium (TMPA), hexadecyltrimethylammonium (HDTMA), cetyltrimethylammonium (CTMA)).[70] The use of Gemini surfactants, characterised by the presence of both aromatic rings and alkyl chain, was also reported for the remediation of water containing pollutants such as bisphenol, *p*-nitrophenol and triclosan.[71,72]

Very recently, the removal of methylene blue from aqueous solutions has been carried out by using Fe_3O_4-multiwalled carbon nanotubes–bentonite composite material.[73]

The anion exchange capacity of clays can be exploited by using physical (*i.e.* thermo-activation processes) and chemical modifications devoted to modifying the interlayer properties of these materials. Chemical activation includes metal or surfactant impregnation and amine grafting. All these methods have, as a general scope, the enrichment of the clay's surface with positive charges that can be exploitable to interact with anions. The results of these modification methods on nitrate removal have been recently reviewed.[74] Clay modification for the removal of anionic dyes was also recently discussed.[75,76]

Magnetic and mechano-chemical modifications of clays have also been proposed for improving the recovery of clays after toxic dye adsorption and/or to improve their adsorption capacity.[77] In the same review, the influence of different physico-chemical properties of modified clays (*i.e.* surface area, particle dimensions, morphology, electrical charges, zeta potential, charge density and swelling properties) on the adsorption of synthetic dyes while varying several parameters such as pH, ionic strength, dye concentration, contact time, and temperature, were reported.

Clays treated in acid media and then modified with polymers, surfactants (both anionic and cationic) or materials derived from the combination of clays with magnetic species and polymers and intercalated surfactants and polymers have been proposed for the recovery of heavy metals and inorganic ions, organic dyes, antibiotics, phenolic compounds.[78–80]

Polymer-amended bentonites for application as barriers to limit the contaminants' diffusion in solids have been recently reviewed, with particular emphasis on the different types of modification and application fields.[81]

These composite materials have generally excellent impermeability properties that are related to the formation of

Table 2 Most representative examples of intercalation compounds based on clays, ZrP and LDHs for the removal of environmental contaminants. The reviews are not reported

Material	Preparation	Mechanism of pollutant removal	Pollutants removed	Maximum adsorption capacity	Ref.
Synthetic saponite clays	Hydrothermal synthesis followed by Na^+ ion exchange	Ion-exchange	La^{3+}, Gd^{3+} and Lu^{3+}	Gd^{3+}: 46.94 ± 1.71 mg g^{-1} La^{3+}: 45.21 ± 1.12 mg g^{-1} Lu^{3+}: 54.89 ± 1.31 mg g^{-1} From simulated freshwaters: Gd^{3+}: 49.48 ± 1.98 mg g^{-1}	56
HNTs modified with Fe_2O_3	HTNs modified by sol gel method	Electrostatic attraction, ligand exchange, and Lewis acid–base interactions	Phosphate anions	Maximum ads capacity: 5.46 mg g^{-1}	62
Fe_2O_3/attapulgite	Ultrasonic co-precipitation method	Adsorption, electrostatic interactions	Arsenite (As^{III})	*ca.* 150 mg As(III) per g Fe	63
Zero valent iron/kaolin	Fe(III) reduction method	Adsorption, reduction	Pb(II)	440 mg g^{-1}	64
Zero valent iron/PILC	Chemical reduction procedure on PILC	Adsorption, reduction	Nitrates	—	65
Zero valent iron/MMT	Impregnation	Adsorption, reduction	Pb(II)	—	66
Organo-modified MMT clays	Ion exchange	Adsorption, π–π interaction and hydrophobic affinity	Bisphenol A	Maximum adsorption: 222.2 mg g^{-1}	71
Organo-modified MMT clays	Ion exchange with gemini surfactants	Surface adsorption and intraparticle diffusion	*p*-Nitrophenol	81.30 mg g^{-1} (for sample modified with 1,3-bis(dodecyldimethyl-ammonio)-2-hydroxypropane dichlor-ide (BDHP))	72
Fe_3O_4-MWCNT-bentonite	*In situ* growth process	Physical adsorption	Methylene blue (MB)	MB adsorption: 48.2 mg g^{-1}	73
Organo-modified paligorskite and sepiolite	Grafting process	Adsorption mechanism *via* hydrophobic interaction and/or hydrogen bonds	Methylene blue (MB) and metanil yellow (MY)	60.00 and 59.78 mg g^{-1} for grafted sepiolite, for MB and MY, respectively	76
Organo-bentonite (AOBent)/ sodium (SA) composite	Intercalation of sodium alginate in activated organo-bentonite	Hydrophobic interactions	Methylene blue (MB) and methyl orange (MO)	414 mg g^{-1} for MB and 116 mg g^{-1} for MO	79
Organo-modified acid-treated bentonite	Acid treatment and ion exchange with surfactants	Surface adsorption and intraparticle diffusion	2,4,5-Trichlorophenol (TC)	TC: 200.6 mg g^{-1}	80
Organo-modified montmorillonite PILCs	Grafting process	Ion exchange and coordination interactions	Co^{2+} ions	Co^{2+} ions: 60 mg g^{-1}	86
AlCr-pillared clays	One pot hydrothermal methods and ion exchange	Physical adsorption	Benzene	Benzene: 48.3 μmol g^{-1}	87
ZrP nanoparticles	$ZrOCl_2$, H_3PO_4 and aqueous Tritron X-100 surfactant	Column separation, ion-exchange	Radioanalytical separation of the no-carrier-added ^{137m}Ba from ^{137}Cs	Cs^+ = 2.593 meq g^{-1}	91
α-ZrP flower-like	$ZrOCl_2$, $8H_2O$, Na_3PO_4, at 80 °C for 96 h	Electrostatic interaction and ion-exchange	^{90}Sr from high-level liquid waste	Sr^{2+} = 293.43 mg g^{-1}	92
ZrP-SO_3H	ZrP exfoliation, grafting of (3-mercaptopropyl)trimethoxysilane, oxidation	Column separation, surface chemical adsorption	^{90}Sr from high-level liquid waste	Sr^{2+} = 183.21 mg g^{-1}	94
γ-ZrP	—	Ion-exchange	Rare earth metal cations	0.06–0.10 mol per mol of γ-ZrP	95
γ-ZrP	$ZrOCl_2{\cdot}8H_2O$, $NaH_2PO_4{\cdot}H_2O$ and NaF ground in an agate mortar, 120 °C for different times	Ion-exchange	Selective adsorption of Cs^+	Cs^+ removal efficiency >98%	96
$K_2Zr(PO_4)_2$	Solid-state reaction using ZrO_2 and KPO_3 (750 °C for 24 h)	Ion-exchange	Separation of ^{90}Sr from nuclear waste	Sr^{2+} = 603 μmol g^{-1}	97
$Zr(NaPO_4)_2{\cdot}H_2O$	$ZrOCl_2{\cdot}8H_2O$, Na_2HPO_4 and NaF were ground in an agate mortar. Heated to 120 °C for 24 h.	Ion-exchange	Heavy metals such as Pb^{2+}, Cu^{2+}, Cd^{2+}, and Tl^+	Highly toxic Tl^+ = 1036 mg g^{-1}	98

Table 2 *(Contd.)*

Material	Preparation	Mechanism of pollutant removal	Pollutants removed	Maximum adsorption capacity	Ref.
α-Zr-$(NH_4PO_4)_2{\cdot}H_2O$	$ZrOCl_2{\cdot}8H_2O$, $(NH_4)_2HPO_4$ and NaF were ground in an agate mortar. Heated to 120 °C for 24 h.	Ion-exchange	Pb^{2+} and Cu^{2+}	Pb^{2+} = 398 mg g^{-1} Cu^{2+} = 144 mg g^{-1}	99
AM-ZrP, AM = 4-amino-benzo-18 crown 6	Intercalation of AM in α-ZrP preintercalated with butylamine	Complexation by AM	^{90}Sr generated in the nuclear fuel cycle	Sr^{2+} = 320.16 mg g^{-1}	100
M-ZrP, M = melamine	Preparation of melamine phosphate (MP). Precipitation reaction between MP and $ZrCl_4$ to obtain M-ZrP	Chelation by M	Pb^{2+}	Pb^{2+} = 1000 mg g^{-1}	101
γ-ZrP-*p*-aminoazobenzene	Intercalation of the azo compounds into γ-ZrP	Ion-exchange and complexation by *p*-aminoazobenzene	Lanthanoid elements	Lanthanoid elements = 370 mg L^{-1} on average	102
Zirconium phenylenediphosphonate-phosphate	Hydrothermal synthesis (120 °C for 4 days) of $ZrOCl_2{\cdot}8H_2O$, $C_6H_4(PO_3H_2)_2$ and phosphoric acid solution	Ion-exchange	Nd^{3+}, Tb^{3+}	Nd^{3+} = 99% of uptake Tb^{3+} = 98% of uptake	103 and 104
GO-Zr-P	Addition of zirconium chloride to the GO suspension under sonication	Chemisorption, mainly through surface complexation	Pb^{2+}, Cd^{2+}, Cu^{2+}, Zn^{2+}	Pb^{2+} = 363.42 mg g^{-1} Cd^{2+} = 232.36 mg g^{-1} Cu^{2+} = 328.56 mg g^{-1} Zn^{2+} = 251.58 mg g^{-1}	105
Fe_3O_4@ZrP	$ZrOCl_2$, $(NH_4)_2HPO_4$, sodium lauryl sulphate and Fe_3O_4 nanoparticles were stirred for 3 h at room temperature	Chemical adsorption	Hg^{2+}	Hg^{2+} = 181.8 mg g^{-1}	106
ZrP@MPS, MPS = mesoporous polystyrene	MPS was immersed into ethanol solutions containing $ZrOCl_2$, followed by evaporation. The beads were incubated with H_3PO_4 for 24	Highly specific inner-sphere coordination of nanoconfined γ-ZrP	Pb^{2+}	Pb^{2+} = 180 mg g^{-1}	107
PVA/ZrP PVDF membrane	PVA and zirconium ions could be coated onto the PVDF membrane through crosslinking reactions with glutaradehyde. The Zr/PVA modified membrane was immersed into the phosphate solution	Ion exchange	Pb^{2+}	Pb^{2+} = 121.2 mg g^{-1}	108
Amorphous-ZrP	Solutions of $ZrCl_4$ and H_3PO_4 were mixed, the precipitated solid was allowed to stand over night	Ion exchange	Nd^{3+}, Dy^{3+}	Nd^{3+} = 0.610 meq g^{-1} Dy^{3+} = 0.628 meq g^{-1}	109
Hydrophilic cellulose-α-ZrP	Dispersion of nano-sized a-ZrP was sprayed onto the surface of the pure cellulose membranes under vacuum filtration	Electrostatic attraction between the heavy metal ions and the high-negatively charged membrane's surface, ion exchange	Pb^{2+}, Ni^{2+}, Cu^{2+}, Zn^{2+}	Cu^{2+}, Zn^{2+}, Ni^{2+}, Pb^{2+} = removal efficiency of 97.0, 98.0, 99.5, and 91.5%, respectively	110
Chitosan-ZrP	Chitosan and ZrP solution was mixed and kept in stirring condition for 24 h	Electrostatic interactions	Cr^{6+}, reactive blue-21 (RB-21), reactive red 141 (RR-141), rhodamine-6G (Rh-6G)	Cr^{6+} = 311.53 mg g^{-1} RB-21 = 457 mg g^{-1} RR-141 = 435.1 mg g^{-1} Rh-6G = 438.6 mg g^{-1}	111
Gelatin-ZrP	Sol–gel method	Ion exchange	Selective adsorption of Cd^{2+}	Cd^{2+} removal efficiency >96%	112
ZrP monolith	$ZrOCl_2{\cdot}6H_2O$, HCl, glycerol, poly(ethylene glycol), polyacrylamide, H_3PO_4	Electrostatic interactions	Adsorption of Ag^+, Cs^+, Sr^{2+}, Zn^{2+}, Cu^{2+}, Pb^{2+}, Cd^{2+}, Fe^{3+}	Percentage of all cations adsorption% >92%	113
ZrP nanoflake	$ZrOCl_2$ in ethanol, HCl, H_3PO_4, stirred thoroughly for 24 h at 60 °C	Strong inner-sphere complexation achieved by Zr–F bonds	Fluoride scavenging	F^- = 55.7 mg g^{-1}	114

Table 2 *(Contd.)*

Material	Preparation	Mechanism of pollutant removal	Pollutants removed	Maximum adsorption capacity	Ref.
C_3N_4-ZrP	α-ZrP nanoparticles and C_3N_4 colloid was dispersed in deionised water and ultrasonicated. The mixture was stirred at 80 °C for 3 h	Photodegradation	RhB	RhB degradation efficiency = 99.95%	115
ZrP/BMIMCl, BMIMCl = 1-*n*-butyl-3-methylimidazolium chloride hybrids	Exfoliated ZrP was acid treated mixed with BMIMCl under ultrasonication	Physical and chemical absorption	CO_2	CO_2 capture capacities = 0.73 mmol g^{-1} at 60 °C	116
MgAl-MoS_4-LDH	$(MoS_4)^{2-}$ was intercalated in MgAl-NO_3 *via* ion exchange reaction	Chemisorption with the adsorption mechanism *via* M–S bonding	Selective removal of Cu^{2+}, Pb^{2+}, Ag^{+}, and Hg^{2+}	Hg^{2+} = 500 mg g^{-1} Ag^{+} = 450 mg g^{-1}	117
MgAl-CMC, CMC = carboxymethylcellulose	Coprecipitation at low supersaturation of LDH in the presence of CMC	Chemisorption	4-Methyl-, 4-propyl- and 4-benzylparaben	4-Methylparaben = adsorption capacity >70%	118
Cu–Zn oxide/Cu–Zn aluminate	CuZnAl-LDH decomposed to CuZn oxide/CuZn aluminate pre-catalyst. Electrochemical reduction to generates CuZn alloy	Electrochemical CO_2 reduction reaction	CO_2	Faradaic efficiency of 88.5% for the conversion of CO_2 to C_{2+} products	123
(LDH/FAS)$_n$-PDMS, FAS = formamidine sulfinic acid, PDMS = poly(dimethylsiloxane)	Self-assembly of LDH, FAS, followed by spray-coating with PDMS layer	Synergy of enhanced solubility, diffusivity and chemical affinity for CO_2 in the sub-nanometre channels	Separation of CO_2	Maximum CO_2 selectivity factor (CO_2/CH_4): 62	124
Vertically aligned graphene sheets membran	Antifreeze-assisted freezing technique	Solar thermal purification	Cr^{3+}, Pb^{2+}, Zn^{2+}, Ni^{2+}, Cu^{2+}	Removal efficiency 99.5%	125
Au/Pt/g-C_3N_4	Calcination-photodeposition technique	Plasmonic photocatalys	Tetracycline hydrochloride (TC)	93.0% of TC degraded in 3 h	126

specific bentonite/polymer intercalated and exfoliated structures. Their applicability as a barrier can be exploited in the presence of inorganic salts, heavy metal species and organic contaminants.

Biochar (BC)/clay composites have been also proposed for the adsorption of both inorganic (*i.e.* heavy metals such as Cs, Cr(VI), Zn, nitrates, NH_4^+...) and organic contaminants (*i.e.* dyes, antibiotics, herbicides...) in soil and water.[82]

BCs are very often produced through low-cost methods and have the potential capability for the removal of environmental contaminants. The combination of BC with clay mineral has been therefore proposed in the literature to improve the SSA and thus the adsorption efficiency of BC. These composites can be obtained essentially by using pre-treatment[83] or post-treatment methods.[84] From reports in the literature it emerges that the synergic combination of clays and BC allows low-cost materials with better capacities for water and soil remediation with respect to the parent constituents to be obtained, because of improved specific surface area and high porosity, chemical, thermal and mechanical stability.

The synthesis steps together with physico-chemical properties, data related to toxicity, and the regeneration ability of various types of modified clay for environmental purposes have been recently reviewed.[78]

The use of pillared clays for environmental applications also deserves some comment.

Among the different pillaring agents, inorganic ligands such as hydroxo and chloro ligands, metal complex ions with organic ligands and polyhydroxy cations (such as $AlCl_3{\cdot}6H_2O$, $ZrOCl_2{\cdot}8H_2O$) metal ions, metal complexes or neutral particles (such as silica sol particles) are reported. The presence of metal oxide pillars (formed upon the calcination step) in the interlamellar space of clays results in a modification of the thermal and hydrothermal stability of the clays. The use of pillared clays for environmental applications has been recently reviewed.[85] Applications include the removal of heavy metals from wastewaters,[86] the adsorption of VOCs and gases such as methane, ethane, benzene, CO_2 coming from industrial activities,[87] and catalytic applications.

Aerogels derived from clays, characterised by a porous microstructure, have been proposed in the last decade for their interesting thermal retardant and adsorption properties that are associated with low toxicity, low cost, and unique structural properties. In particular, montmorillonite (MMT)-based aerogels have been studied to improve their adsorption properties by modifying their preparation method (Fig. 7). A concise review on the possible use of MMT-aerogels for environmental remediation recently appeared in the literature.[88]

2.2 Environmental applications of ZrP

Due to the presence of hydroxyl groups with acid properties, ZrP shows a high ion exchange capacity, metal ion selectivity and fast kinetics. Its ability to withstand heat, ionizing radiation, acidic media and an oxidizing environment makes it a very promising material for sorption of radioactive and heavy metal cations.[89,90] Special attention has been paid to the

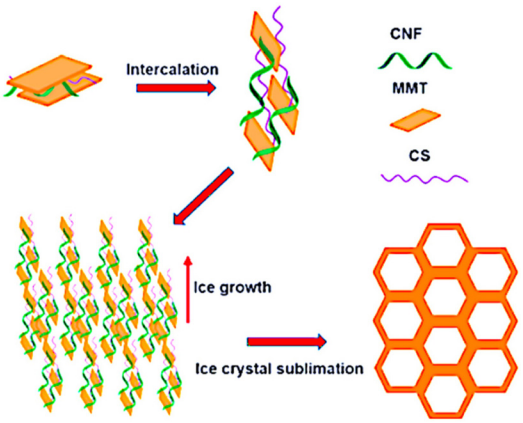

Fig. 7 Schematic view of the mechanism of the pore structure formation of the MMT–chitosan aerogels. Reproduced with permission from ref. 88, Copyright 2023 Elsevier.

removal of Cs^+ and Sr^{2+} cations (because ^{90}Sr and ^{137}Cs are present in high-level liquid nuclear waste) and highly toxic Pb^{2+}, Hg^{2+} and Cd^{2+} ions. With the increasing use of rare earth elements in industry in recent times, the need to remove them from contaminated water is also increasing.

The ion exchange capacity of ZrP nanoparticles was found to increase with decreasing particle size.[91] Recently, there were some attempts to affect Sr^{2+} adsorption by changing particle morphology (nanoflowers[92] or spheres[93]) or by surface modification with SO_3H groups.[94] Another approach is based on the use of ZrP derivatives with greater gallery height, such as γ-ZrP (for Cs^+ and rare earths),[95,96] α-$K_2Zr(PO_4)_2$ (for Sr^{2+}),[97] α-$Na_2Zr(PO_4)_2{\cdot}H_2O$ (for heavy metal cations)[98] and α-$(NH_4)_2Zr(PO_4)_2{\cdot}H_2O$ (for Pb^{2+} and Cu^{2+}).[99] The sorption capacity of ZrP can be enhanced by its combination with organic molecules with high metal affinity. For example, intercalation of 4-aminobenzo-18-crown-6, which has a strong complexing ability for Sr^{2+}, into α-ZrP leads to a composite with excellent stability under acid and radioactive conditions and an adsorption capacity exceeding other similar zirconium adsorbents.[100] Melamine zirconium phosphate,[101] synthesized by the addition of zirconium tetrachloride to melamine phosphate solution, was tested for adsorption of Pb^{2+}, Hg^{2+} and Cu^{2+}. The sorption ability of γ-ZrP towards rare earth metals can be significantly enhanced by intercalation of *p*-aminoazobenzene.[102] Clearfield's group reported the enhanced ability of mixed zirconium phenylenediphosphonate-phosphate to take up Nd and Tb cations, where the selectivity for Nd^{3+} depends on the amount of phosphate.[103,104]

Graphene oxide-zirconium phosphate nanocomposite, prepared by dropwise addition of zirconium chloride to a sonicated graphene oxide suspension, with the subsequent addition of NaH_2PO_4, was tested for the removal of Pb^{2+}, Cd^{2+} and Cu^{2+} cations.[105] Fe_3O_4@ZrP nanocomposite, prepared in a similar way, was efficiently used for Hg^{2+} removal from solution.[106] An important benefit of this adsorbent is its simple separation by magnetic power.

The abovementioned adsorbents based on ZrP were tested for metal exchange in batch experiments at a laboratory scale, but these materials are not suitable for column operation on a large scale. To overcome this problem, composites with various polymers were tested. α-ZrP and γ-ZrP encapsulated into mesoporous polystyrene[107] or zirconium phosphate-modified polyvinyl alcohol-poly(vinylenedifluoride) membrane[108] demonstrate promising sorption performance for Pb^{2+}. Amorphous ZrP nanoparticles exhibit promising adsorption capacity and selectivity for Dy and Nd cations.[109] Recently, biocomposites of ZrP with cellulose,[110] chitosan,[111] and gelatin[112] were used for the sorption of heavy metals. Another elegant way to make ZrP suitable for large-scale application is the preparation of ZrP monoliths combining micro- and mesopores.[113]

All the abovementioned examples describe ZrP as a cation adsorbent, but α-ZrP nanoflakes were also used as a fluoride scavenger. Preferable fluoride adsorption was ascribed to the formation of Zr–F complexes.[114]

Another relevant source of environmental pollution is organic dyes. Organic dyes may have a positive charge or a group that can be protonated and intercalated by zirconium phosphate, but ZrP can also act as a support for species with photocatalytic properties such as titania, silver nanoparticles or graphene oxide and carbon nitrides.[90] Rhodamine B was successfully decomposed using zirconium phosphate/silver/silver halide[27] or an α-ZrP carbon nitride composite[115] under ultraviolet light. A ZrP-gelatin nanocomposite was able to decompose methylene blue and Fast green under solar light.[112] A ZrP-chitosan nanocomposite was used for the sorption of several types of organic dye (copper phthalocynanine dye – reactive blue-21, azo dye reactive red 141, and xanthene dye-rhodamine-6G), and can also serve as a catalyst for the hydrogen peroxide degradation of these dyes.[94]

Co-assembled ZrP nanosheet/1-*n*-butyl-3-methylimidazolium chloride hybrids could serve as highly efficient CO_2 absorbents.[116]

2.3 Environmental applications of LDHs

As has been known for decades, ion exchange compounds present properties to trap or release species according to their affinity. Such chemical speciation is often imposed by the charge of the species present. However, the uptake of ions incompatible with the exchanger is possible, as shown by an elegant approach which circumvents the problem of charge compatibility by first intercalating a complexing guest species MoS_4^{2-} into LDH with respect to ions of opposite charge such as Co^{2+}, Ni^{2+}, $Zn^{2+} < Cd^{2+} \ll Pb^{2+} < Cu^{2+} < Hg^{2+} < Ag^+$, ranked by their selectivity of removal by the hybrid LDH.[117] Due to its high adsorption capacity, LDH/MoS_4^{2-} is very well positioned for the remediation of water polluted by heavy metals. The interlayer species of LDHs may be useful for the adsorption of contaminants. This is the case of carboxymethylcellulose (CMC) as an interlayer anion to sorb parabens.[118] Interestingly, the hybrid CMC LDH can be regenerated at least five times without any pronounced loss of efficiency. LDHs can

photocatalytically degrade pollutants such as dyes and nitro-compounds, as recently reviewed.[119] Specifically Fenton, photoFenton, and electro-Fenton reactions are of great interest in advanced oxidation processes to decontaminate wastewater, and LDH-based frameworks including FeMn as cation in their composition compare well with other materials such as spinel-type, perovskite-type or MOF.[120]

In addition to wastewater treatment and the role played by LDH as a scavenger, some new trends are appearing concerning CO_2 photocatalytic reduction[121] and capture for limiting anthropogenic pollution.[122]

To face the new challenge of carbon neutrality, one possibility is to decompose CO_2 electrocatalytically, as this also addresses the energy domain by producing a renewable fuel.[123] A template based on Cu–Zn–Al LDH is used to form Cu–Zn oxide/Cu–Zn aluminate, uniformly dispersed thanks to the cation dispersion within the LDH pristine precursor. The optimised composition is found to reach a faradaic efficiency of 88.5% for the conversion of CO_2 to C_{2+} products. Membranes composed of LDH nanosheets self-assembled with formamidine sulfinic acid and formed with poly(dimethylsiloxane) are reported to perform effectively for selective CO_2 separation.[124]

The shaping of graphene and the complementary plasma-assisted oxidation of material open the way to novel devices as efficient membranes for water treatment, thanks to the optimised diffusion pathway and hydrophilic feature improving the capillary effect for effective water infiltration. This can clearly be considered more as water insertion rather than a true intercalation reaction.[125]

Concerning water cleaning, metal/g-C_3N_4 can display enhanced photocatalytic activity thanks to plasmonic effects in the heterostructure with noble metals such as gold and/or platinum. These catalysts can be used for the degradation of antibiotic residues and other pharmaceutical contaminants that induce negative environmental effects,[126] but this once again consists more of surface reactions than intercalation.

3. Applications of intercalation materials for health purposes

Intercalation compounds are being increasingly studied for their possible application in the health domain. Once their biocompatibility has been verified, it is indeed possible to consider inorganic structures that can provide solutions for the release of active ingredients, for antimicrobial or bone reconstruction activity, or even more generally for theranostic applications, as reviewed recently.[127,128]

Representative applications of intercalation compounds based on clays, ZrP and LDHs for health purposes are described below, and then summarised in Table 3.

3.1 Applications of clays in the health domain

Nanoclays are attracting increasing interest for their enhanced therapeutic effects. Indeed, their biocompatibility, the bacteriostatic or bactericidal activity exhibited by some clays,[129] and their high surface area, adsorption capacity, ability to serve as carrier for therapeutics and to release drugs in a controlled manner make them ideal candidates for applications in biomedical engineering,[130] tissue engineering and regenerative medicine,[131] wound healing,[132] drug delivery systems,[133] bioimaging[134] and 3D bio inks for use in medical purposes.[135] It is worthy to note that attention has also been paid to commercially available clays such as LAPONITE® in the field of health, as reviewed by Tomás *et al.*,[136] owing to their purity but above all due to their high aspect ratio derived from their 25 nm disk-shaped particles. The most promising use of clays and clay-based nanocomposites is in the field of drug delivery systems,[137–141] including antimicrobial,[142,143] antibiotic,[143,144] and anti-cancer[145] as well as theranostic[146,147] and antihistamine treatments.[148]

Montmorillonite (MMT) clay has been frequently utilised as a drug vehicle due to its high specific surface area, excellent cation exchange capacity and biocompatibility. To avoid flocculation of MMT under physiological conditions the surface has to be modified. For example, PEGylated chitosan (PEG-CS) adducts can be used to modify the clay surface, thus leading to a good dispersion in a serum-containing environment (Fig. 8) as well as resulting in interesting drug carriers.[145]

Examples of the uses of PCHs derived from MMT clays for drug delivery applications are also reported. PCHs prepared using montmorillonite as starting material are interesting supports for methotrexate (MTX) encapsulation due to the superior drug encapsulation efficiency (EE) with respect to MMT parent clay (EE values higher than 97% for PHCs compared with EE = 45% for MMT clay).[134] It was also observed that PCH hosts can influence drug release in relation to their pore architecture. The drug is released in a proportion higher than 70%, whereas from MMT parent clay only 9.7% of MTX is released.[134]

Halloysite is one of clay minerals showing maximum efficiency as a nano drug carrier, and demonstrates exceptional biocompatibility and low cytotoxicity when tested for use in cell cultures and tissues.[149,150] Moreover, thanks to its size, the inner lumen can accommodate molecules of interest, while small drug molecules can be filled into the wall interlayer spaces and molecules can be either adsorbed or covalently bonded on the outer surface. As different interactions can occur, an initial drug burst can start from the outer surface and be followed by a sustained release of the drug from the inner surface (lumen) owing to a slower leakage.

Drugs can be loaded into HNTs from saturated drug solutions or a melt of low water-soluble drugs. Pan *et al.*[151] loaded vancomycin, a drug used for serious Gram-positive bacterial infections, into the internal cavity of halloysite by using different mass ratios of vancomycin and halloysite *via* sonication and vacuuming, obtaining a solid with high antibacterial activity against *S. aureus* and *B. streptococcus*. The use of HNTs allowed the preparation of a local antibiotic delivery system without the need for a particularly energy-consuming process, thus allowing the controlled release of molecules beneficial for targeted applications.

Table 3 Most representative examples of intercalation compounds based on clays, ZrP, LDHs and graphene for health purposes. The data contained in reviews are not reported

Material/substrate	Active species	Procedure to introduce the active species	Application	Biological system	Ref.
Palygorskite and HNTs clays	$Eu(DBM)_3(H_2O)_2$ (HDBM dibenzoylmethane)	PEI grafting and further modification with terpyridine derivatives to introduce an antenna species. The Eu complex is introduced *via* a ligand exchange reaction.	Bioimaging applications	Tested for bioimaging with HeLa cell line Promising in applications as targeting cancer cells and in drug delivery systems	134
Amino-modified clays in liposomes	Budesomide	Polyelectrolytes, aminoclay and Eudragit® S100, were assembled directly on the liposomal surface *via* a layer by layer deposition	Drug-releasing carriers	Colon-targeted delivery system	138
Porous clay heterostructures based on MMT clay	Methotrexate (MTX)	MTX encapsulation	MTX delivery systems, chemotherapy	Potential use of PCHs/MTX in pharmaceutical field for cancer treament	139
Organo-clay (alkylammonium on MMT)	Methylene blue (MB) (as a model drug)	Intercalation process	Drug delivery system	Thermo-sensitive hydrogel based on Pluronic and nanoclay potentially exploitable as injectable systems and as a long-term delivery system	141
MMT clay	Tetracycline hydrochloride	Ion exchange process	Antibacterial effect	Gram-positive and Gram-negative bacteria	142
MMT clay in polylactide matrix	Gentamicin and neomycin	Intercalation process	Antibacterial activity	*Escherichia coli* (*E. coli*)	143
Smectite clays	Ciprofloxacin	Ion exchange	Antibacterial Effect	*E. coli* and *Staphylococcus aureus* (*S. aureus*)	144
MMT modified with PEGylated chitosan (PEG-CS)	Doxorubicin (DOX)	Impregnation	Drug delivery	TRAMP-C1 cells epithelial cell line	145
Fe-MMT clay	Photosensitizer TPCI	Ion exchange, intercalation	Photodynamic therapy, antibacterial effect, wound healing	*E. coli*, *Pseudomonas aeruginosa* (*P. aeruginosa*) and *S. aureus* *In vivo* antibacterial and wound healing assay	146
HNTs	Vancomycin	Physical dispersion, sonication, vacuuming	Local drug delivery system	HL-60 cell lines (*in vitro* cell cytotoxicity) Antibacterial activity on *S. aureus* and *B. streptococcus*	151
HNTs	Ciprofloxacin and polymyxin B sulfate	Physical dispersion, sonication, vacuuming	Wound dressing, antimicrobial activity	*S. aureus* and *P. aeruginosa*	153
HNTs	Thymol	Cryogel synthesis	Wound healing	—	154
HNTs	DOX	Impregnation	Drug delivery	MFC mouse gastric cancer cells	156
HNTs	Icariin	Vacuum loading method	Bone tissue engineering	*In vitro* osteogenic differentiation	161
HNTs-poly[bis(carboxyphenoxy) phosphazene]	Amoxicillin and marine sponge	Inclusion and adsorption	Antibacterial and antibiofilm coating for the Ti–6Al–4 V screw for dental implantation	*S. aureus*, *E. coli*, *Porphyromonas gingivalis*	164
HNTs	Deferoxamine	Inclusion	3D-printed scaffold to realise the coupling regeneration of blood vessels and bones	Bone marrow mesenchymal stem cells (BMSCs), human umbilical endothelial cells (HUVECs)	165
Saponites	Gd-complexes	Cation exchange	Diagnostic MRI and theranostics	—	166
Saponites	Gd-(or Y^{3+})TETA-monoamide chelates	Cation exchange	Diagnostic MRI and theranostics	—	167

Table 3 *(Contd.)*

Material/substrate	Active species	Procedure to introduce the active species	Application	Biological system	Ref.
Fe_3O_4@HNTs	Lanthanide complex, iron oxide	One-step hydrothermal process combined with the coupling grafting method	Bioimaging and biological applications in human hepatic adenocarcinoma cells and diagnostic MRI	Human hepatic (LO2) and human hepatic adenocarcinoma (HepG2) cell line, MRI was performed *in vivo* in tumour-bearing rabbits	168
Fe_3O_4 – LAPONITE®	Fe_3O_4	Schikorr reaction	Localised magnetic hyperthermia (MH) and diagnostic MRI	Human glioblastoma cells (U87EGFRvIII) and human foreskin fibroblasts (HFF), MRI was performed *in vivo* in rodent brain	169
γ-ZP	Alendronate	Exfoliation, topotactic exchange	Drug delivery capable of promoting bone mineralisation and inhibiting bone resorption	Human bone osteosarcoma (MG-63)	171
ZrP	DOX	Intercalation	Drug delivery of anticancer drugs	MCF-7 and MDA-MB 231 cancer cell lines, MCF-10A cells, human prostate cancer PC3	173 and 174
ZrP	Curcumin	Adsorption	Drug delivery of anticancer drugs	MDA-MB-231 breast cancer cell lines	175 and 176
Fe_3O_4/α-ZrP	5-Fluorouracil folate acid-chitosan-rhodamine6G complex	Exfoliation, intercalation	Deliver anticancer drug for tumour optical imaging and therapy	A549, HeLa and HEK293 cells	177
α-ZrP	Methylene blue	Cation exchange	Photodynamic therapy	MDA-MB-231 breast cancer cell	178
α-ZrP/carboxymethylcellulose	Chlorhexidine	Intercalation, solvent casting	Antimicrobial and antibiofilm wound dressings	HDF human dermal fibroblast cells (HuDe) and human keratinocyte (NCTC2544) cell lines	179
α-ZrP	Ag^+	Cation exchange	Antimicrobial	*E. coli* Saos-2 (Sarcoma osteogenic) cell line	180
α-ZrP/poly(lactide-*co*-glycolic acid)	NorA efflux pump inhibitors	Intercalation, solvent casting	Antibiofilm composites	*S. aureus* *Staphylococcus epidermidis*	181
α-ZrP	Bromfenac	Exfoliation, adsorption	Drug delivery of anti-inflammatory drug	—	182
α-ZrP	Caffeine	Exfoliation, intercalation	Topical application	—	183
α-ZrP or LDH/poly (ethyleneoxideterephthalate)/poly (butyleneterephthalate)	Gentamicin, ciprofloxacin	Intercalation, melt-blending, melt extrusion	3D scaffolds for bone infection prevention and tissue regeneration	*S. epidermidis*, *P. aeruginosa* cytotoxicity on human mesenchymal stromal cells (hMSCs) osteogenic differentiation capacity of hMSCs	184
Alg-Cu MOF-LDH beads	DOX	Co-precipitation and *in situ* growth method.	Drug delivery system for cancer therapy	L929 non-cancerous cells, MCF-7 human breast cancer cells	188
MgAl-LDH/poly(ε-caprolactone)	LDH	Electrospinning technique	Nanocomposite scaffolds	Mouse adipose derived stem cells (mADSC)	194
Graphene oxide	Graphene oxide nanosheets	Intercalation/exfoliation (Hummers' method)	Antimicrobial surface coatings	*E. coli*	195

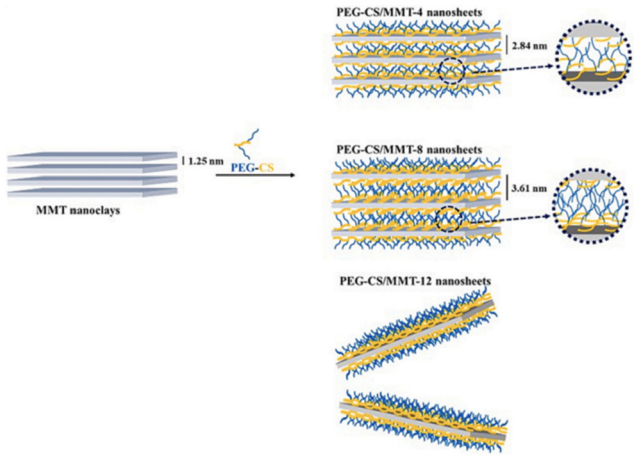

Fig. 8 Microstructures of PEG-CS/MMT nanosheets with various PEG-CS/MMT. Reproduced with permission from ref. 145, Copyright 2022 Elsevier.

Norfloxacin, an anti-microbial agent, was loaded within HNT and then embedded with chitosan to prepare bio-nanocomposite films.[152]

Antimicrobial gelatin-based elastomer nanocomposite membranes loaded with ciprofloxacin and polymyxin B sulfate-loaded halloysite nanotubes were formed for wound dressing applications.[153] A combination of ciprofloxacin (characterised by a broad-spectrum antimicrobial activity inhibiting both Gram-negative and Gram-positive bacteria) and polymyxin B-sulfate, with a narrow spectrum of activity mainly against Gram-negative bacteria, aimed at having a co-operative anti-infection effect. It was reported that HTNs play a dual role of enhancing the matrix tensile strength and slowing down the release rate of highly dissoluble drugs.

Recently, the formation of a hybrid system based on biocompatible poly 2-hydroxyethyl methacrylate (pHEMA) and thymol-loaded halloysite was reported for application as portable wound dressing to protect injured skin;[154] the antibacterial, antifungal and anti-inflammatory properties of thymol make this compound interesting for the development of devices for tissue repair. Also in this case, HTNs were exploited to entrap the thymol in the lumen to ensure a sustained release of the drug.

Doxorubicin (DOX) is widely used as a chemotherapeutic drug, owing to its effectiveness in combating numerous types of cancers. However, as some serious side effects have been witnessed, DOX delivery vectors based on different hosts were developed, as recently reported.[155] In this regard DOX was, for example, loaded into HNTs and then encapsulated by soybean phospholipid (LIP) to form HNTs/DOX/LIP.[156] The optimal DOX loading efficiency was higher than 22%. A pH-responsive release property with fast drug release under acidic conditions (pH = 5.4) was evidenced by *in vitro* drug release testing, and *in vivo* experimental results revealed that such compounds exhibit a significantly higher inhibitory efficacy on the growth of mouse gastric cancer cells than free DOX at the same drug concentration.

The development of chitosan/halloysite/graphitic-carbon nitride compounds for quercetin targeted delivery was performed to overcome the weak hydrophilicity, chemical instability and low bioavailability of quercetin which, however, presents anti-inflammatory, antiviral and mainly anticancer effects. The combination of carbon nitride (g-C_3N_4), which is similar in structure to graphene, has a low biological toxicity and can be metabolised in biological systems,[157] with HNT and chitosan to form hydrogels, followed by a loading of quercetin using a water-in-oil-in-water emulsification process to attain quercetin sustained-release, leads to a remarkable encapsulation loading and loading efficiency (up to 86%) and the formation of a pH-responsive behaviour that minimizes the side effects of quercetin by controlling its burst release at neutral conditions. These new nanocomposites also revealed a significantly higher cytotoxicity against breast cancer cells in comparison with quercetin as a free drug.

The reported examples suggested that clays can be exploited as nano containers for applications in drug delivery, antimicrobial materials, self-healing polymeric composites, and regenerative medicine that entail time-extended functions.

In the field of tissue engineering, which aims to develop biological substitutes that replace and restore structural and functional properties of tissues, HNTs are also arguably the most promising candidates, as besides all their already-mentioned properties, their unique structure can significantly increase the mechanical and chemical stability of tissue engineering scaffolds.[158–160] Applications for bone tissues,[161] cartilage repair,[162] implants,[163] dental fillings,[164] and tissue scaffolds[165] underline all the advantages of HNTs. As interesting results, in the field of orthopedic implants, Dharmaraj *et al.*[163] mentioned the antibacterial, anti-cancer and osteosarcoma cell growth-impediment properties of composites prepared by electrodeposition of strontium-halloysite nanotubes (Sr-HNT)/lanthanum cerium-substituted hydroxyapatite composite coatings on titanium used as implant materials. In addition, an anti-corrosion effect of this new type of coating was also revealed. A 3D-printed scaffold with a sequential delivery platform was also formed starting from deferoxamine-loaded HTNs, bone morphogenetic protein-2 and poly(L-lactide-*co*-glycolide)/b-tricalcium phosphate solution with the aim of realizing the coupling regeneration of blood vessels and bones.[165] These new composites promote cell–scaffold interactions by enabling cell adhesion, spreading, and differentiation *in vitro*, and also enhance subcutaneous ectopic bone formation *in vivo via* the synergistic effect of deferoxamine and bone morphogenetic protein-2, therefore paving the way for new treatments for bone defects.

The inherent properties of clay minerals, such as fluorescence and paramagnetism, enable their utilisation in biomedical imaging techniques. Functionalised clay nanoparticles have been developed as contrast agents for magnetic resonance imaging (MRI), providing improved imaging resolution and targeting capabilities. Paramagnetic clays have been obtained by introducing, in the interlayer space of saponite clays, Gd^{3+}-complexes by a classical ion exchange reaction. It

was pointed out that the interactions of the complexes with the saponite layers have a certain influence on both the local rotational dynamics and exchange process of water molecules between the internal Gd^{3+} coordination sphere and the bulk.[166,167] Clay-based lanthanide polymer nanocomposites were for example formed,[135] starting from polyethyleneimine and a lanthanide complex attached onto the surface of halloysite or palygorskite, leading to nanocomposites exhibiting both intense red emission under visible light excitation, long luminescent lifetime as well as high quantum yields, and improved photoluminescence stability. The photoluminescent and magnetic properties of multifunctional halloysite nanotube Fe_3O_4@HNT-polyethyleneimine-Tip-Eu(dibenzoylmethane)$_3$ were also reported,[168] one interesting feature being that these composites displayed superparamagnetic behaviour and also worked as a magnetic resonance imaging (MRI) contrast agent *in vitro* and *in vivo*. The Schikorr reaction, which involves the oxidation of layered $Fe(OH)_2$, was used to prepare superparamagnetic Fe_3O_4 – LAPONITE®.[169]

3.2 ZrP-based compounds for health applications

The discovery that ZrP is harmless to the body, since it is highly hemocompatible, not toxic, and not associated with any metabolic function, has paved the way for using these compounds in the nanomedicine field.[170] The insertion into ZrP of molecules of biological interest can occur *via* ion-exchange reactions between the acid protons of the solid and the molecular cations, intercalation of basic molecules and topotactic exchange of phosphate by phosphonate groups. This last strategy is mainly applied in γ-ZrP. In this context, the alendronate, a *gem*-bisphosphonate used to treat bone diseases, was immobilised in γ-ZrP by topotactic exchange to obtain a drug delivery system.[171] When the biological molecules are particularly bulky a preintercalation step in alpha type is mandatory to enlarge the interlayer region; a strategy to avoid this step is the use of θ-ZrP, a hydrated form of α-ZrP with six water molecules per formula unit. Otherwise, one-pot intercalation can be achievable by starting from a gel of nanometric α-ZrP in ethanol or propanol.[172] The alcohol present in the interlayer region keeps the layers far enough apart to promote the intercalation of bulky species.

Particular attention has been paid to delivering chemotherapeutic drugs loaded in nanocarriers, to target cancer cells and minimize drug side-effects. DOX, one of the most used anticancer drugs, is highly toxic to cancer cells and to normal tissue, causing several adverse effects. To overcome these drawbacks, DOX was intercalated into θ-ZrP to obtain a compound (DOX@ZrP) with a drug loading of 34.9 wt%. Two-dimensional ^{31}P NMR studies showed that DOX is intercalated as a neutral molecule and interacts with the ZrP layers by hydrogen bonds among protonated phosphate groups and the amine and –OH groups of DOX, involving also hydration water molecules. The release of DOX from DOX@ZrP in simulated body fluid at pH 7.42 is prolonged, extending to 11–14 days. Cellular studies showed that DOX@ZrP samples were favoured for cellular uptake and cytotoxicity in MCF-7 and MDA-MB 231 cancer cell lines compared with free DOX. *In vitro* studies in MCF-7 and MCF-10A cells showed that ZrP nanoparticles are able to promote the uptake of DOX@ZrP by endocytosis, especially in cancerous cells.[173] The biocompatibility of DOX@ZrP was improved by surface functionalisation with monomethyl-poly (ethylene glycol)-monophosphate, and cytotoxicity towards human prostate cancer PC3 cells was about 20% higher than free DOX.[174]

Kalita *et al.* prepared nanometric zirconium pyrophosphate, having the dimension of about 48 nm, by a sonochemical method in the presence of cetyltrimethylammonium bromide as surfactant followed by calcination at 700 °C. The nanoparticles were used to immobilise curcumin ((1*E*,6*E*)-1,7-bis(4-hydroxy-3-methoxyphenyl)-1,6-heptadiene-3,5-dione), a model drug with anti-inflammatory, antioxidant and anti-tumour properties. The loading of the drug in the composite (ZP-CUR) was 11.5 wt%. The *in vitro* drug release from ZP-CUR was pH sensitive and was higher at pH 5 than pH 7.4, making the composite suitable for delivering and releasing the drug in the acidic intracellular environment of tumour cells. The cytotoxicity studies of free curcumin and of ZP-CUR, performed on MDA-MB-231 breast cancer cell lines, showed an enhancement of the cytotoxic effect of the formulate curcumin as compared with the native form.[175]

Antitumour drugs lack specificity for tumour cells, thus exhibiting high cytotoxicity also for normal cells. The use of magnetic nanoparticles (Fe_3O_4), anchored to the nanocarrier, allows, through an external magnetic field, the delivery and anchoring of the drug in a specific site, enhancing the drug activity. In this context, Kalita *et al.* extended their work with curcumin-loaded amorphous zirconium phosphate as the shell for magnetite core nanocarriers.[176] The release profile and cytotoxicity in MDA-MB-231 cell lines was comparable to those of ZP-CUR previously described.

To improve targeted drug delivery to tumour cells, nanocarriers conjugated with folate seem to be a promising strategy since the cancer cells over-express folate receptors. Magnetite nanoparticles and 5-fluorouracil (5-FU) were intercalated in α-ZrP preintercalated with butylamine. The compound obtained was covered with a folate acid-chitosan-rhodamine6G (FA-CHI-R6G) complex to obtain the system 5-FU/Fe_3O_4/α-ZrP@FA-CHI-R6G (Fig. 9). The presence of R6G, which acts as a fluorescent probe, suggests the nanocomposite as a promising material for bioimaging. Moreover, the nanocomposite has no cytotoxic effects on A549 cells, interacts with FA-positive HeLa cells while the FA-negative HEK293 cells show little uptake of the nanomaterials, and shows a sustainable 5-FU release.[177]

An alternative to the use of chemotherapeutic drugs for cancer treatment is photodynamic therapy (PDT), which is based on photoactivation of a photosensitizer able to form cytotoxic reactive oxygen species. The photosensitizers, as the antitumour drugs, have nonspecific interactions that also cause damage to normal cells.

The photosensitizer methylene blue (MB) was intercalated in α-ZrP by cation exchange with the acid protons. The ZrP-MB

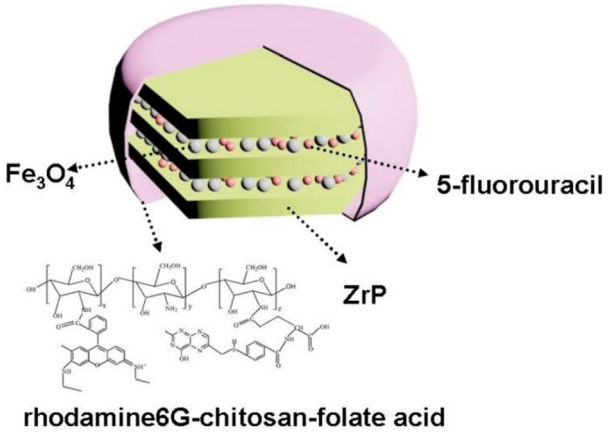

Fig. 9 Schematic representation of the 5-FU/Fe_3O_4/α-ZrP@CHI-FA-R6G nanocomposites. Reproduced with permission from ref. 177, Copyright 2015 American Chemical Society.

nanoparticles were able to deliver MB to MDA-MB-231 breast cancer cells and to reduce the toxicity of pure MB in a dark experiment. PDT efficacy on ZrP-MB-treated MDA-MB-231 cells was enhanced upon MB intercalation. The nanoparticles protect the MB from the reduction to "leuco-methylene blue" in biological systems that generally limits the clinical use of MB, and release it preferentially in cancer cells due to their acidic microenvironment.[178]

Several active molecules were intercalated starting from the gel of nanometric α-ZrP in ethanol. Chlorhexidine (CLX), a broad spectrum antimicrobial agent, was intercalated starting from the gel of nanometric α-ZrP, reaching a drug loading 50 wt%. ZrP(CLX) was used as a filler of sodium carboxymethylcellulose to prepare films as potential wound dressings. The films showed antimicrobial and antibiofilm activity. Moreover, *in vitro* cytotoxicity tests of the films in HDF human dermal fibroblast cells (HuDe) and human keratinocyte cell lines (NCTC2544) showed reduced cytotoxicity of CLX due to its prolonged release, which maintains a low CLX concentration.[179] Silver NPs were immobilised on α-ZrP *via* the H^+/Ag^+ ion-exchange process followed by thermal treatment. The Ag-enriched α-ZrP showed antimicrobial activity against *Escherichia coli*.[180]

The intercalation properties of the gel of nanometric α-ZrP in ethanol were exploited to intercalate potent in-house *S. aureus* NorA efflux pump inhibitors. The intercalation compounds were used as fillers of poly(lactide-*co*-glycolic acid). The composites showed an antibiofilm activity comparable to that of film containing ZrP intercalated with thioridazine, a NorA and biofilm inhibitor.[181]

An alternative way to promote the interactions between the α-ZrP surface and biomolecules is the use of a gel of zirconium phosphate obtained by exfoliation with propylamine and regenerated with HCl. The gel was able to immobilise the anti-inflammatory drug bromfenac (BFS)[182] and caffeine,[183] a central nervous system stimulant. The compound ZrP-BFS showed a BFS release profile that was pH dependent; a complete release of BFS was obtained at pH 7.

Finally, a ZrP-gentamicin intercalation compound was used as a filler of a thermoplastic polymer and the composite was processed *via* high-temperature melt extrusion into 3D scaffolds. The antibiotic, released in a sustained manner, maintained its activity against Gram+ and Gram− bacteria, and the scaffolds were not cytotoxic towards hMSCs cells and did not prevent their osteogenic differentiation.[184]

3.3 Applications of LDHs for health purposes

LDHs are also studied today for their possible biomedical applications.[185] Their trapping and release ability is important regarding the delivery of drugs or bioactive molecules as well as their ease of handling and scale-up.[186] Accommodation of bioactive molecules within the LDH host structure leads to bioactive hybrid materials that can be efficient in administration and associated with low cytotoxicity, this triggered by the pH of human fluids to precisely target a site. They may be of use for delivering cosmeceutical, natural or synthetic biomolecules. When considering the formed bio-hybrid composite, it may be considered as a win–win partnership, the host LDH protecting the bioactive molecule from aggressive media while the guest maintains the layered structure until its ingress out of the LDH cargo. Due to their biocompatibility, LDHs are also studied in terms of clinical translation of their bio-activity and bio-reactivity concerning orthopaedic diseases and other bone tumours.[187]

LDH-supported MOFs loaded in alginate beads, a pH-sensitive biopolymer extracted from seaweed,[188] have been prepared to control the release of DOX for cancer therapy. *In vitro* cytotoxicity in MCF-7 cells (human breast cancer cells) showed that the loaded beads have a higher cytotoxic effect than the free DOX. The higher DOX activity may be due to the presence of the Alg coating and the controlled DOX release into cancer cells. Other reviews report the combination of organic polymer with LDH as well.[189] From *in vivo* assays it is demonstrated that such bio-hybrid composites containing bioactive guests are of interest in pharmaceutical and medical applications, and that review more specifically focused on drug delivery and tissue engineering regarding skin and bone therapies. For the latter, it is observed that LDH composites can be safely integrated into living matter as well as being stimuli-responsive when exposed to collagen. Of course, other naturally occurring clay minerals such as montmorillonite and halloysite may also be combined with biocompatible polymers to carry the active ingredient of interest in drug delivery or in tissue engineering.[190] In the latter case, the bio-hybrid composites are found to induce cell adhesion and proliferation, helping in regenerating skin damage. It is indeed a set of 2D materials which can be considered as bio-platforms in theranostics (therapeutic and diagnostic) when endowed with bio-functionalities,[191] as found in the critical and cutting-edge review discussing the current challenges and their future research directions regarding such applications in human health.

Chemotherapeutic and gene-therapeutic functions for hetero-structured layered nanohybrids using clays (in general) have been recently reviewed, underlining the possibility of drug–clay nanohybrids being relevant for drug administration and release.[192]

Similarly, another review reports such carriers for gene-LDH focusing on intercellular gene uptake mechanisms and their intracellular ingress, but also with imaging and targeting functions.[193]

Other health domains may be relevant, such as tissue and bone engineering, where LDH dispersed into fibers of poly(ε-caprolactone) (PCL) by the electrospinning technique are studied to mimic tissue-engineering scaffolds.[194] The study reports the viability, proliferation, and adipogenic differentiation of mouse adipose-derived stem cells and shows that LDH-enriched electrospun PCL scaffolds with high porosity increase cell adhesion and proliferation, suitable for application in soft tissue regeneration.

More specifically for bone healing, 3D additive-manufactured scaffolds made with biodegradable polymers and LDH intercalated with ciprofloxacin have been designed to present possible antibiotic release for antimicrobial activity to prevent infection in the case of an open bone fracture or in implant surgery. Incorporation of LDH-ciprofloxacin into the scaffolds did not affect the viability of human mesenchymal stromal cells (hMSCs) or prevent their osteogenic differentiation.[184] An intercalation/exfoliation procedure following Hummers' method led to the synthesis of graphene oxide (GO). Consecutively to this intercalation process, the so-obtained materials exhibited a size-dependency of GO antimicrobial activity. The defect quantity is correlated to the size/specific surface area of the GO, giving guidelines for future development of graphene-based antimicrobial surface coatings.[195]

Tunable surface properties, transparency, electronic capabilities, biocompatibility and outstanding flexible mechanical properties make graphene a promising material for biomedical applications such as biomedical electronic devices or implants. However, the material generally called "graphene" is, in fact, a large variety of carbon-based materials. Following these considerations, graphene-based materials used for biomedical applications must be regarded while paying particular attention to the characterisations defining them. Consequently, some "rules" must be established concerning the synthesis considerations and the possible biomedical applications depending on the characteristics of graphene. If graphene can be obtained by the CVD procedure, intercalation using Hummers' method can lead to GO and then reduced graphene oxide (RGO) interesting for health purposes.[196]

4. Applications of intercalation materials in polymer science

Clays and graphene have been extensively studied as fillers of polymeric composite, and the research has been summarised in several reviews and thematic books. Therefore, to avoid redundancy, discussion of the main aspects related to polymeric composites based on these layered materials is entrusted to the most recent reviews and books.[197–204]

Here, the latest examples of the use of ZrP and LDHs as a filler of polymeric composites are reported. Table 4 summarises the recent applications of intercalation compounds based on ZrP and LDHs for polymer science.

4.1 ZrP compounds for polymer science applications

Zirconium phosphate nanosheets, the size and thickness of which can be precisely controlled, are suitable nanofillers for improving the anti-corrosion properties of polymeric coatings.[205] It was shown that improved barrier properties, caused by self-assembly of ZrP nanosheets, are mainly responsible for the increased corrosion resistance of ZrP/epoxy resin (Fig. 10),[206] ZrP/polyurethane[207] or ZrP/polybenzoxazine coatings.[208]

Zirconium phosphate is also a possible candidate for flame retardancy applications, due to its high thermal stability and phosphorus content. In addition, the aspect ratio and size of the nanoparticles can be controlled by the choice of synthesis and exfoliation method. Exfoliated ZrP significantly enhanced the thermal stability and flame retardation behaviour of polybenzoxazine by improving the stability of the char layer and reducing the amount of flammable gases (Fig. 11).[209]

Hybrid platelet nanostructures formed by the self-assembly of ZrP, melamine and cyanuric acid significantly improved the flame retardancy and crystallinity of polyamide6 (Fig. 12).[210] Acrylamide-modified ZrP/polyacrylate nanocomposite was prepared *via in situ* polymerization and the effect of ZrP (dimension of *ca.* 120–160 nm) amount and the quality of its dispersion on flame retardancy was described.[211] When *ca.* 0.5 wt% of modified ZrP was added, a decrease of nanoplatelets dimensions was visible because of the exfoliation process (Fig. 12B-B′). An increase in ZrP content to 3 wt% leads to the formation of large aggregates (Fig. 12C-C′) that might have a negative effect on the mechanical properties and flame retardancy of the composite.

ZrP nanoplates modified with hexachlorocyclotriphosphane and melamine in polyvinyl alcohol composite improve the yield and graphitization of char residues, and make the char more stable, compact and continuous, inhibiting the underlying polymer from coming into contact with heat and oxygen.[212] The synergistic effect between polyphosphazene and α-ZrP in polypropylene composites improved the thermal stability of the matrix and increased the amount of char yield in comparison with polypropylene containing either only polyphosphazene or only ZrP.[213] Organo-modified ZrP combined with another traditional flame retardant agent aluminium hydroxide leads to improved flame retardancy of ethylene vinyl acetate, low-density polyethylene/ethylene-vinyl acetate copolymer, and polystyrene.[214,215] Hierarchical graphene-confined zirconium phosphate nanosheets were used to improve the thermal conductivity, mechanical properties and flame resistance of cellulose nanofiber aerogels.[216]

Table 4 Most representative examples of intercalation compounds based on ZrP and LDHs in polymer science. The reviews are not reported

Filler	Polymeric matrix	Preparation method	Purpose	Performances	Ref.
α-ZrP	Polydopamine (PDA)	*In situ* polymerisation	Composite epoxy coating	Corrosion protection (improved anticorrosion performance with I_{corr} of 6.60×10^{-9} A cm^{-2}, which are one order of magnitude lower than that of blank epoxy coating)	206
α-ZrP	Polyurethane	*In situ* polymerisation	Advanced coatings	Reduction of *ca.* 40% in H_2O permeability, anti-corrosion protection	207
α-ZrP	Polybenzoxazine	Thermal curing process	Flame retardance	Improved thermal stability and flame retardancy (49.3% peak of heat release rate reduction (PHRR) with respect to pure matrix)	209
α-ZrP	Polyamide6	Melt blending	Flame retardance	Improved flame retardancy (*ca.* 83% PHRR with respect to pure matrix)	210
α-ZrP	Polyacrylate	*In situ* emulsion polymerisation	Flame retardance	Improved flame retardancy. LOI (limited oxygen index) value of 25% against 23% of pure PPA	211
α-ZrP	Poly(vinyl alcohol)	Solution blending	Flame retardance	Improved graphitization of char residues and thermal stability	212
α-ZrP	Polypropylene	Melt blending	Flame retardance	Improved formation of char residues and higher thermal stability with respect to pure matrix. LOI value *ca.* 26% *vs.* 17% in pure PP matrix	213
Organo-modified ZrP LDH (m-ZrP)	Ethylene vinyl acetate	Melt blending	Flame retardance	Incorporation of mZrP/LDH mixture into EVA/ATH composite resulted in a reduction in thermal stability but improved the char yield at 750 °C. EVA composites exhibited improvement in fire retardancy (decreased PHRR, THR, TSP and the enhanced char yield): LDH was more effective than mZrP in char formation; on the other hand, mZrP showed a 73% reduction in PHRR, which was more efficient than LDH (58% reduction in PHRR)	214
Organophilic α-ZrP	Low-density polyethylene and ethylene–vinyl acetate (LDPE/EVA) hybrid	Bradender extrusion	Flame retardance	Improved flame retardancy. LOI value of the composite *ca.* 32 against 20.3 of the pure polymer	215
Hierarchical graphene-confined zirconium phosphate nanosheets (ZrP/RGO)	Cellulose-based aerogels	Unidirectional freeze-casing technique	Thermal insulation, flame retardance, mechanical properties	Thermal conductivity (18 mW m^{-1} K^{-1}), and high LOI (33.5) as well as very low PHRR (14.1 kW m^{-2})	216
α-ZrP	PET film	Layer-by-layer (LbL) assembly	Oxygen barrier properties	Oxygen transmission rate (OTR) reduced from 57 to 0.87 cc per m^2 per day for the best composite material.	218
Organo-modified MgAl LDHs	Polybutylene succinate (PBS)	Melt extrusion	Viscoelastic properties, rate of hydrolysis, photodegradation, antibacterial activity	Small rate of hydrolysis, photostability, biocide activity, chain extension is obtained using a combination of LDHs-L-ascorbate and LDH-3-(4-hydroxyphenyl)propionate	222
LDH-RA (RA = rosmarinic acid), LDH-SA (SA = salicylic acid)	Low-density polyethylene (LDPE)	Two-step melt compounding procedure	Antibacterial activity	LDPE/MgAl-RA was selective and strongly inhibitory toward *S. aureus*, LDPE/ZnAl-SA inhibited the growth of *E. coli and S. aureus*	223
LDH MgAl-D (D = 3-(3,5-di-*tert*-butyl-4-hydroxyphenyl)propionic acid)	Polypropylene	Solvent mixing method	Anti-aging	Good stability against thermal aging, low migration of molecules out of the PP films	224
LDH MgAl-AO (AO = Irganox 1010)	Polypropylene	Solvent mixing method	Anti-aging	LDH-AO significantly enhances long-term performance of LDH/PP composites against thermal/thermo-oxidative degradation	227

Table 4 *(Contd.)*

Filler	Polymeric matrix	Preparation method	Purpose	Performances	Ref.
LDH ZnAl-HxDy (H = 4-oxo-4-((2,2,6,6-tetramethylpiperidin-4-yl)amino)butanoic acid; D = 3-(3,5-di-*tert*-butyl-4-hydroxyphenyl) propionic)	Polypropylene	Solvent or extrusion mixing	Anti-aging	The co-intercalated hybrid materials are found to decelerate the oxidative degradation for PP	228
LDH CaAl-HnMn′ (M = Irganox 1425; H = hindered amine light stabilizer)	Polypropylene	Solvent casting method	Anti-aging	Higher overall resistance against thermal degradation and photooxidation	229

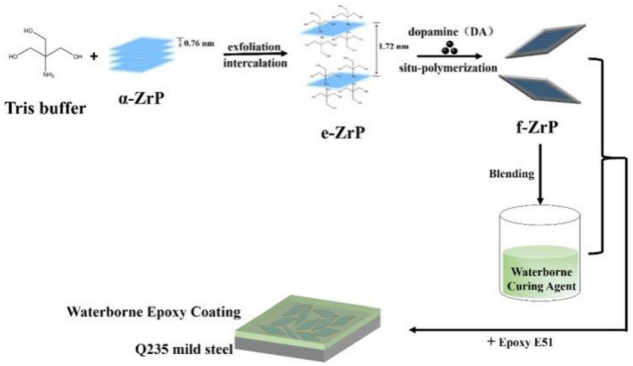

Fig. 10 Exfoliation and functionalisation process of α-ZrP (f-ZrP) and the preparation of f-ZrP/WEP nanocomposite coatings. Reproduced with permission from ref. 206, Copyright 2020 Elsevier.

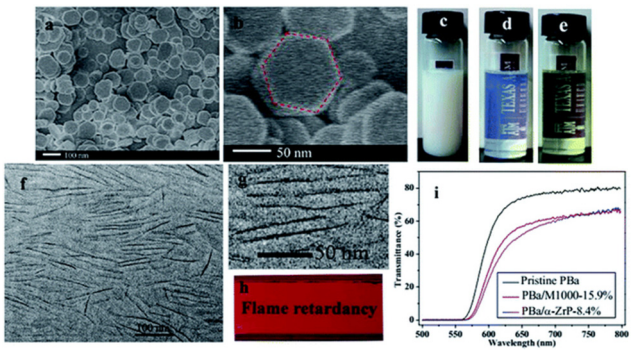

Fig. 11 (a) and (b) SEM of original α-ZrP, (c) original α-ZrP in acetone, (d) exfoliated α-ZrP in acetone, (e) Ba/α-ZrP-8.4% in acetone, (f) and (g) TEM of PBa/α-ZrP-8.4% nanocomposites, (h) photographic images of PBa/α-ZrP-8.4% nanocomposites and (i) light transmission spectra of samples. Adapted with permission from ref. 209, Copyright 2016 Royal Society of Chemistry.

The use of α-ZrP nanosheets as a nano-filler in polymers for food packaging applications is very limited; some examples are given in Ghanbarzadeh's *et al.* review.[217] A combination of graphene and ZrP nanosheets with different two-dimensional scales results in a synergistic ordering effect that increased the tortuosity of the permeation path for oxygen molecules to travel through the PVA nanocomposite films and significantly decreased their oxygen permeability. A similar nano-bricks wall architecture was obtained through layer-by-layer deposition of polyacrylic acid, poly(dimethyl diallyl ammonium chloride), and α-ZrP nanosheets onto polyethylene terephthalate film (Fig. 13).[218] The oxygen transmission decreased exponentially with the number of the deposited quadlayers (consisting of three repeat units of polyacrylic acid, poly (dimethyl diallyl ammonium chloride) and α-ZrP), and the transparency of the film was not significantly reduced; therefore, this composite film shows great potential for application in packaging.

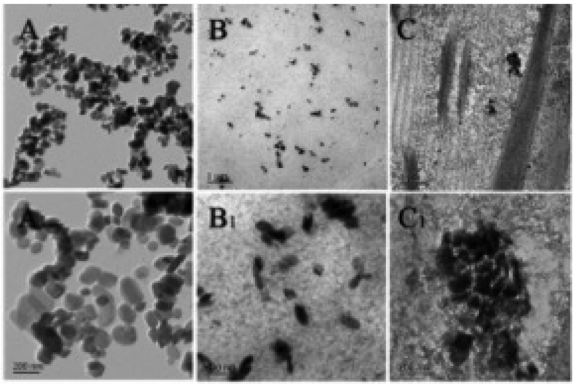

Fig. 12 TEM images of ZrP/polyacrylate nanocomposite. A-A′: α-ZrP, B-B′ and C-C′: PPA/AM-ZrP-1 composites with 0.5 and 3 wt%, respectively. Reproduced with permission from ref. 211, Copyright 2017 Royal Society of Chemistry.

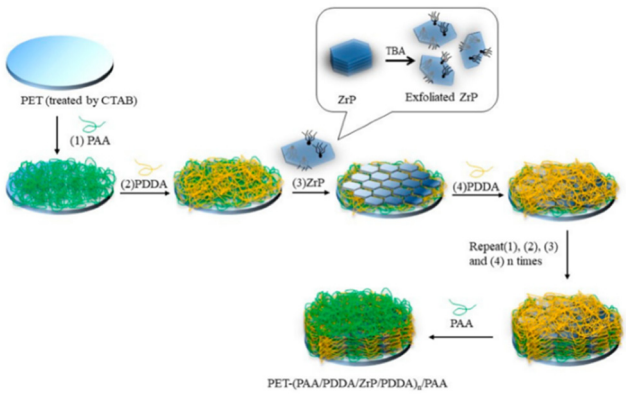

Fig. 13 Schematic of the layer-by-layer (LbL) assembly for polyacrylic acid (PAA)/poly(dimethyl diallyl ammonium chloride) (PDDA)/zirconium phosphate (ZrP)/PDDA quadlayers. PET: polyethylene terephthalate; TBA: tetrabutylammonium; CTAB: hexadecyl trimethyl ammonium bromide. Reproduced with permission from ref. 218, Copyright 2018 MDPI.

4.2 LDHs-based compounds for polymer science

LDHs are often used as a polymer filler as they can be customised to accommodate functionalities such as fire retardancy, UV-stabilization, biocide, water or moisture permeability or repellant (increase of the hydrophobicity by the presence of platelets organo-modified by surfactants) while providing the expected barrier-effect by the enhancement of tortuosity coming from the high mechanical modulus of the anisotropic platelets.[219] More specifically, they may be of interest in food packaging by increasing the shelf life of food products and adding organoleptic and nutritional value.[220] LDHs contribute to stabilizing or enhancing certain properties of PVC[221] or PBS.[222] In the latter case, with organic anions interleaved into LDH fillers (L-tyrosine (TYR), L-tryptophan (TRP), L-ascorbate (ASA) and 3-(4-hydroxyphenyl)propionate (HPP)), it was possible to demonstrate antibacterial properties for the films in combination with a high chain extension effect suitable for polymer processability. When LDH intercalated with salicylate and rosmarinate anions is dispersed into LDPE, the formed polymer nanocomposites present strong antibacterial activity against *Staphylococcus aureus* and antioxidant properties altogether suitable for packaging materials.[223]

Furthermore, LDH has been used as a barrier to protect antioxidants from migrating out of the polymer.[224] Hindered phenolic antioxidants have gained widespread recognition and application in enhancing the heat resistance and oxidative aging performance of polypropylene (PP) composites.[225] However, the use of low molecular weight antioxidants poses certain challenges. These antioxidants have a greater tendency to volatilise, migrate, and be extracted from PP or PP-based products. Such behaviour directly diminishes the anti-thermal oxidative aging efficacy of PP and its composites, and additionally presents a risk of contaminating food or drugs when used in packaging.[226] LDHs are highly desirable as antioxidant protection materials due to their adjustable compositions (M^{2+} and M^{3+}) within the host sheet, replaceable interlayer anions (A^{n-}) in the interlayer region, and adaptable charge density (M^{2+}/M^{3+} ratio). Consequently, it is plausible to inhibit the migration of antioxidants utilizing host–guest interactions and supramolecular forces by incorporating low molecular weight antioxidant species into the interlayer gaps of transparent LDHs. The 3-(3,5-di-*tert*-butyl-4-hydroxyphenyl)-propionate anions (AO, one-fourth of the most used antioxidant in industry, Irganox 1010) were intercalated into Mg_2Al-LDH, thus leading to AO-LDH samples by a one-step synthesis. Moreover, AO-LDH/PP composites were obtained through a solvent washing method. It was proved that the intercalation of AO anions between LDH led to an improvement of the antioxidative performance of PP composites. A barrier effect was offered by the host sheet of MgAl-AO-LDH thus allowing greater migration resistance than that of AO/PP composite.[227] Based on theory, the composition of the host layer and the interlayer guests in the intercalation structure antioxidants was controlled to achieve homogeneity of the resulting compounds, leading to the construction of a class of supramolecular intercalated structure antioxidants with anti-migration properties, such as the single-intercalated MgAl-HALS-LDH photostabiliser[228] and the co-intercalated CaAl-HxMy-LDH anti-aging agent.[229]

As far as corrosion inhibition is concerned, LDHs are also found to be of interest in polymer coatings for metal substrates such as magnesium alloys (AZ91D, an alloy of interest but lacking stability when exposed to the marine environment) using the so-called self-healing behaviour of LDH cargo, since the release is triggered by corrosion.[230] LDHs can be mixed with other frameworks as exemplified in one article,[231] where the idea is to build a 3D fir tree-like hierarchical architecture by utilizing pulsed plasma electrolysis with LDHs and a zeolitic imidazolate framework to protect the magnesium alloy substrate.

5. Remarks and outlook

This perspective has focused on the role played by intercalation chemistry as an evaluable tool for the design and synthesis of materials to meet some of the challenges of our

century. Particular attention has been paid to developing catalysts for producing clean energy, converting molecules derived from biomass into value-added products, degrading pollutants, materials for environmental remediation, systems for use in medicinal chemistry and for the preparation of polymeric composites.

As far as heterogeneous catalysts are concerned, the layered materials here reviewed provide sustainable catalyst sources with several advantages: easily recoverable and highly reusable, economical, and efficient catalytic potential under mild conditions. The intercalation chemistry allows us to obtain solids with transition metal species, with great interest for catalytic purposes. Metals can be intercalated as inorganic polycations within the interlayer space of clay (PILCs) or as cations or cationic complexes in ZrP. Transition metals can be inserted as constituents of the LDH layers. All these possibilities allow to obtain catalysts with improvements in specific surface area, thermal stability, dispersion of the active phase and sometimes catalytic performance thanks to specific interactions of the active species with the functional groups of the layer or their confinement in the interlayer region. Layered materials have been used as systems capable of favouring the growth of metallic nanoparticles upon intercalation of metallic ions followed by reduction in a confined environment. Otherwise, preformed metallic NPs can be immobilized on material surface. The confinement of NPs improves their resistance to cleavage and agglomeration as well as their catalytic activity. In addition, the immobilisation of the NPs favours their recovery and reuse. Recently, superior catalytic performance has been achieved by combining different materials to obtain heterostructures (*i.e.* TiO_2/clays, HNT/MOFs, *etc.*).

The ability of layered materials to intercalate ionic or molecular species has made them very good candidates as solid adsorbents for the removal of pollutants. The literature survey indicated that clays, ZrP and LDH can be successfully modified to improve the adsorption ability towards environmental contaminants, thus making them potential candidates for wastewater treatments. The presence of intercalated functional groups (classically leading to an increase of the basal spacing, modification of textural properties and surface hydrophobicity) and, in some case, the increase in swelling ability are key factors affecting the adsorption properties of intercalated compounds and leading to an improvement of adsorption properties with respect to raw materials.

ILCs can be also active as photocatalysts for pollutant degradation. This property is very often achieved in the case of compounds containing metal oxide particles, that can be thus stabilised from the layered matrices.

In this sense, efforts must be made in searching for sustainable synthetic methods (especially in terms of time and production costs) for layered materials-based intercalation compounds. Few methods are, for instance, related to ultrasound-accelerated synthesis. As an example, environmentally safe low-cost adsorbents can indeed be obtained also starting from natural clays by using microwave-assisted heating methods.[232] Another emerging green and powerful synthesis is mechanochemistry, due its scalability and tunability. This technique has great potential for the environmentally friendly production of layered materials for applications in the sustainable energy and environmental sectors.[233]

Most of the papers in the recent literature are related to the use of ILCs for the removal of pollutants from simulated matrices. Since the solution pH and the presence of interfering ions and/or molecules can interfere with the main adsorption mechanism, the performances of materials must be tested in different conditions (*i.e.* distilled water, groundwater, industrial wastewater, sea water) to assess the real applicability of materials.[234]

Moreover, there are still problems to be solved in the use of materials as catalysts, especially when used to remove pollutants from water. For practical applications, correct monitoring of the species formed during the catalytic reaction, together with the detection of possible toxic intermediates, must be carried out.

For health purposes, the interlayer region of layered materials can be considered as a nanocontainer capable of protecting the bioactive species from light and oxygen. Moreover, the intercalation compounds, suitably modified, can provide targeted delivery of therapeutic species by releasing them upon a specific stimulus (variation of pH, temperature).

Among clays, halloysite is a promising local delivery system that does not require exfoliation or any other complicated energy-consuming process, thus permitting the storage and controlled release of molecules.

The application of zirconium phosphate for drug delivery has not been extensively studied. However, the ability of ZrP to exfoliate in aqueous solution makes this material a good candidate for hosting bulky cations and basic species with therapeutic activity. Attention should be focused on scalable and green syntheses of ZrP, taking into account mechanochemistry. As for LDHs, ILCs have long been considered for the preparation of drug delivery systems. Future opportunities for these materials are related to the modulation of the layer composition, which can be constituted by several metal cations. The correct choice of these intralayer metals (*i.e.* Zn, Ga, Cu, Mg...), which can be released in appropriate media, can produce materials with therapeutic properties. In addition, a new frontier is the possibility of creating defect sites in the LDH layer that can be tailored to the needs of cancer immunotherapy. For photothermal/photodynamic therapy, sonodynamic therapy, and pH-sensitive magnetic resonance imaging, the modulation of defect sites in the crystal structure of LDH enables it to respond sensitively to external stimuli.[235]

Finally, layered materials have been used as nanofillers to improve the thermal stability, mechanical properties of polymers and anti-corrosion properties of polymeric coatings. The inorganic filler, intercalated with active species, absolves to another task that is to impart to the polymer additional properties such as antioxidant and antimicrobial properties.

However, in general, one of the major issues in materials development in many areas is scaling up from the laboratory level to large-scale implementation as an available and affordable commercial solution. The production of large quantities of intercalation compounds means the simplification of prepa-

ration steps, the elimination of toxic solvents/reagents, and reduced production costs. The last of these could be achieved by using waste materials where possible, in accordance with the principles of the circular economy.

The recovery and reuse processes of these adsorbents are not always studied in the literature. Moreover, the fate of recovered pollutants merits additional consideration to develop sustainable and circular economy processes.[234] An interesting example of Cr-based PILCs for the recovery of anionic and cationic species was recently reported in the literature.[236] The study is especially focusing on the possibility of reducing the synthesis time and cost, identifying the optimal conditions for effective adsorption of individual dyes using Cr-pillared clay after statistical analysis through the design of experiments. Moreover, in many cases, we must continue efforts to understand the structure–property relationships. As an example, for PILCs different characterisation techniques are needed to reveal their still unknown properties, thus paving the way for intelligent material design.

Data availability

Manuscript Ms. ref. no.: DT-PER-03-2024-000757 entitled "Recent advances and perspectives for intercalation compounds. Part 2: applications in the field of catalysis, environment and health", authored by Chiara Bisio, Jocelyne Brendlé, Sébastien Cahen, Yongjun Feng, Seong-Ju Hwang, Morena Nocchetti, Dermot O'Hare, Pierre Rabu, Klara Melanova, Fabrice Leroux. No primary research results, software or code have been included and no new data were generated or analysed as part of this review.

Conflicts of interest

There are no conflicts to declare.

Acknowledgements

All co-authors as well as all colleagues from the board of the International Symposium on Intercalation Compounds (ISIC) are warmly acknowledged.

References

1 M. Massaro, R. Noto and S. Riela, *Molecules*, 2020, **25**, 4863.
2 S. Nawaz, M. Ahmad, S. Asif, J. J. Klemes, M. Mubashir, M. Munir, M. Zafar, A. Bokhari, A. Mukhtar, S. Saqib, K. S. Khoo and P. L. Show, *Bioresour. Technol.*, 2022, **343**, 126068.
3 A. Ramli, M. Farooq, A. Naeem, S. Khan, M. Hummayun, A. Iqbal, S. Ahmed and L. A. Shah, in *Frontiers in Bioenergy and Biofuels*, ed. E. Jacob-Lopes and L. Queiroz Zepka, IntechOpen, 2017, vol. 14, pp. 285–308.
4 T. Chellapandi and G. Madhumitha, *Mol. Divers.*, 2022, **26**, 2311–2339.
5 S. Sadjadi, *Appl. Clay Sci.*, 2020, **189**, 105537.
6 Y. Li, X. Yuan, L. Jiang, H. Dai, Y. Zhao, X. Guan, J. Bai and H. Wang, *Environ. Sci.: Nano*, 2022, **9**, 841–866.
7 Y. Zheng, L. Wang, F. Zhong, G. Cai, Y. Xiao and L. Jiang, *Ind. Eng. Chem. Res.*, 2020, **59**, 5636–5647.
8 Y. H. Ahmad, A. T. Mohamed and S. Y. Al-Qaradawi, *Appl. Clay Sci.*, 2021, **201**, 105956.
9 N. M. Sanchez-Ballester, G. V. Ramesh, T. Tanabe, E. Koudelkova, J. Liu, L. K. Shrestha, Y. Lvov, J. P. Hill, K. Ariga and H. Abe, *J. Mater. Chem. A*, 2015, **3**, 6614–6619.
10 F. Carniato, C. Bisio, R. Psaro, L. Marchese and M. Guidotti, *Angew. Chem., Int. Ed.*, 2014, **53**, 10095–10098.
11 F. Carniato, C. Bisio, C. Evangelisti, R. Psaro, L. Marchese and M. Guidotti, *Dalton Trans.*, 2018, **47**, 2939–2948.
12 S. Marchesi, M. Guidotti, L. Marchese, F. Carniato and C. Bisio, *Chem. – Eur. J.*, 2021, **27**(14), 4723–4730.
13 E. M. Serwicka, *Catalysts*, 2021, **11**, 1087.
14 K. Bahranowski, W. Włodarczyk, E. Wisła-Walsh, A. Gaweł, J. Matusik, A. Klimek, B. Gil, A. Michalik-Zym, R. Dula and R. P. Socha, *Microporous Mesoporous Mater.*, 2015, **202**, 155–164.
15 B. Szczepanik, *Appl. Clay Sci.*, 2017, **141**, 227–239.
16 M. Kashif, M. Yuan, Y. Su, P. M. Heynderickx and A. Memon, *Appl. Clay Sci.*, 2023, **233**, 106847.
17 M. C. Dlamini, M. S. Maubane-Nkadimeng and J. A. Moma, *J. Environ. Chem. Eng.*, 2021, **9**, 106546.
18 S. Yoda, Y. Sakurai, A. Endo and T. Miyata, *J. Mater. Chem.*, 2004, **14**, 2763–2767.
19 D. Chen, Q. Zhu, F. Zhou, X. Deng and F. Li, *J. Hazard. Mater.*, 2012, **235–236**, 186–193.
20 L. Chmielarza, A. Kowalczyk, M. Skoczek, M. Rutkowska, B. Gil, P. Natkański, M. Radko, M. Motak, R. Dębek and J. Ryczkowski, *Appl. Clay Sci.*, 2018, **160**, 116–125.
21 M. Pica, *Catalysts*, 2017, **7**, 190.
22 H. Ding, A. Ahmed, K. Shen and L. Sun, *Aggregate*, 2022, **3**, e174.
23 F. Wang, Z. Yuan, B. Liu, S. Chen and Z. Zhang, *J. Ind. Eng. Chem.*, 2016, **38**, 181–185.
24 C. Zhu, Q. Liu, D. Li, H. Wang, C. Zhang, C. Cui, L. Chen, C. Cai and L. Ma, *ACS Omega*, 2018, **3**, 7407–7417.
25 M. Chen, J. Xia, H. Li, X. Zhao, Q. Peng, J. Wang, H. Gong, S. Dai, P. An, H. Wang and Z. Hou, *ChemCatChem*, 2021, **13**, 3801–3814.
26 J. He, Y. Jiang, B. Ding, Y. Wang, H. Qiu, S. Dai, X. Zhao and Z. Hou, *Appl. Catal., A*, 2023, **664**, 119351.
27 M. Pica, M. Nocchetti, B. Ridolfi, A. Donnadio, F. Costantino, P. L. Gentili and M. Casciola, *J. Mater. Chem. A*, 2015, **3**, 5525–5534.
28 M. Pica, S. Calzuola, A. Donnadio, P. L. Gentili, M. Nocchetti and M. Casciola, *Catalysts*, 2019, **9**, 3.

29 Y. Xu, F. Zhou, M. Chen, H. Hu, L. Lin, J. Wua and M. Zhanga, *New J. Chem.*, 2020, **44**, 9793–9801.
30 L. Lin, Y. Wen, L. Li, Y. Tan, P. Yang, Y. Liang, Y. Xu, H. Hu and Y. Xu, *Nanomaterials*, 2022, **12**, 3339.
31 J. Zhou, H. Sun, C. Xu, Z. Wang, H. Zhang, D. Guo, J. Zhang, X. Ji, L. Liu, J. Ma and Z. Tong, *J. Taiwan Inst. Chem. Eng.*, 2022, **138**, 104478.
32 M. V. Ramos-Garcés and J. L. Colón, *Nanomaterials*, 2020, **10**, 822.
33 M. V. Ramos-Garcés, J. Sanchez, D. E. Del Toro-Pedrosa, I. B. Alvarez, Y. Wu, E. Valle, D. Villagrán, T. F. Jaramillo and J. L. Colón, *ACS Appl. Energy Mater.*, 2019, **2**, 3561–3567.
34 M. V. Ramos-Garcés, J. Sanchez, K. La Luz-Rivera, D. E. Del Toro-Pedrosa, T. F. Jaramillo and J. L. Colón, *Dalton Trans.*, 2020, **49**, 3892–3900.
35 J. Sanchez, M. B. Stevens, A. R. Young, A. Gallo, M. Zhao, Y. Liu, M. V. Ramos-Garcés, M. Ben-Naim, J. L. Colón, R. Sinclair, L. A. King, M. Bajdich and T. F. Jaramillo, *Adv. Energy Mater.*, 2021, **11**, 2003545.
36 S. Kumar, A. Yoyakki, A. Pandikassala, R. Soni and S. Kurungot, *Adv. Sustainable Syst.*, 2023, **7**, 2200330.
37 A. Sharma, S. Kumari, S. Sharma, T. Singh, S. Kumar, A. Thakur, S. K. Bhatia and A. K. Sharma, *Mater. Today Sustainability*, 2023, **22**, 100399.
38 J. Wu, Y. Xie, Y. Li, M. Jin, L. Liu, G. Pan, C. Wang and F. Li, *Coord. Chem. Rev.*, 2023, **497**, 215437.
39 B. Sardar and D. Srimani, *Tetrahedron*, 2023, **138**, 133414.
40 Y. Xiao, J. Li, Y. Tan, X. Chen, F. Bai, W. Luo and Y. Ding, *Int. J. Mol. Sci.*, 2023, **24**(19), 14859.
41 C. Gastaldi, C. Taviot-Gueho, C. Guerard-Helaine and C. Forano, *Appl. Clay Sci.*, 2023, **238**, 106931.
42 L. Izquierdo-Aranda, R. Adam and J. R. Cabrero-Antonino, *ChemSusChem*, 2023, **16**, e2023008.
43 U. A. Mohanty, D. P. Sahoo, L. Paramanik and K. Parida, *Sustainable Energy Fuels*, 2023, **7**, 1145–1186.
44 Y. Liu, Y. Guo, Y. Liu, Z. Wei, K. Wang and Z. Shi, *Energy Fuels*, 2023, **37**, 2608–2630.
45 P. R. Chowdhury, H. Medhi, K. G. Bhattacharyya and C. M. Hussain, *Coord. Chem. Rev.*, 2024, **501**, 215547.
46 D. K. Perivoliotis, J. Ekspong, X. Zhao, G. Hu, T. Wagberg and E. Gracia-Espino, *Nano Today*, 2023, **50**, 101883.
47 Y. Liao, R. He, W. Pan, Y. Li, Y. Wang, J. Li and Y. Li, *Chem. Eng. J.*, 2023, **464**, 142669.
48 Z.-Q. Liu, X. Liang, F.-X. Ma, Y.-X. Xiong, G. Zhang, G. Chen, L. Zhen and C.-Y. Xu, *Adv. Energy Mater.*, 2023, **13**, 2203609.
49 R. Dai, C. Dai, S. Hou, Q. He, B. Liu, M. Huang, H. Jiang, M. Li, L. Pan and Z. Guo, *J. Mater. Chem. A*, 2023, **11**, 20383–20407.
50 D. Tyndall, M. J. Craig, L. Gannon, C. McGuinness, N. McEvoy, A. Roy, M. Garcia-Melchor, M. P. Browne and V. Nicolosi, *J. Mater. Chem. A*, 2023, **11**, 4067–4077.
51 A. Zitolo, V. Goellner, V. Armel, M.-T. Sougrati, T. Mineva, L. Stievano, E. Fonda and F. Jaouen, *Nat. Mater.*, 2015, **14**, 937–942.
52 J. Duan, S. Chen, M. Jaroniec and S. Z. Qiao, *ACS Catal.*, 2015, **5**, 5207–5234.
53 M. K. Uddin, *Chem. Eng. J.*, 2017, **308**, 438–462.
54 V. B. Yadav, R. Gadi and S. Kalr, *J. Environ. Manage.*, 2019, **232**, 803–817.
55 S. Manna, P. Das, P. Basak, A. K. Sharma, V. K. Singh, R. K. Patel, J. K. Pandey, V. Ashokkumar and A. Pugazhendhi, *Chemosphere*, 2021, **280**, 130961.
56 S. Marchesi, F. Carniato, M. Guidotti, M. Botta, L. Marchese and C. Bisio, *New J. Chem.*, 2020, **44**, 10033–10041.
57 S. Marchesi, S. Nascimbene, M. Guidotti, C. Bisio and F. Carniato, *Dalton Trans.*, 2022, **51**, 4502–4509.
58 S. Marchesi, C. Bisio and F. Carniato, *RSC Adv.*, 2020, **10**, 29765–29771.
59 T. Zhang, W. Wang, Y. Zhao, H. Bai, T. Wen, S. Kang, G. Song, S. Song and S. Komarneni, *Chem. Eng. J.*, 2021, **420**, 127574.
60 H. Bai, Y. Zhao, X. Zhang, W. Wang, T. Zhang, C. Liu, H. Yi and S. Song, *J. Am. Ceram. Soc.*, 2019, 3908–3922.
61 H. Bai, Y. Zhao, W. Wang, T. Zhang, H. Yi and S. Song, *Ceram. Int.*, 2019, **45**, 17054–17063.
62 D. A. Almasri, N. B. Saleh, M. A. Atieh, G. McKay and S. Ahzi, *Sci. Rep.*, 2019, **9**, 1–13.
63 D. Yao, Y. Shi, H. Pan, D. Zhong, H. Hou, X. Wu, J. Chen, L. Wang, Y. Hu and J. C. Crittenden, *Chem. Eng. J.*, 2020, **392**, 123637.
64 X. Zhang, S. Lin, X. Q. Lu and Z. L. Chen, *Chem. Eng. J.*, 2010, **163**, 243–248.
65 Y. Zhang, Y. Li, J. Li, L. Hu and X. Zheng, *Chem. Eng. J.*, 2011, **171**, 526–531.
66 N. Arancibia-Miranda, S. E. Baltazar, A. García, D. Munoz-Lira, P. Sepúlveda, M. A. Rubio and D. Altbir, *J. Hazard. Mater.*, 2016, **301**, 371–380.
67 N. Ezzatahmadi, G. A. Ayoko, G. J. Millar, R. Speight, C. Yan, J. Li, S. Li, J. Zhu and Y. Xi, *Chem. Eng. J.*, 2017, **312**, 336–350.
68 M. R. Olson, T. C. Sale, C. D. Shackelford, C. Bozzini and J. Skeean, *Groundwater Monit. Rem*, 2012, **32**, 63–74.
69 A. M. Awad, S. M. R. Shaikh, R. Jalab, M. H. Gulied, M. S. Nasser, A. Benamor and S. Adham, *Sep. Purif. Technol.*, 2019, **228**, 115719.
70 Y. Park, G. A. Ayoko and R. L. Frost, *J. Colloid Interface Sci.*, 2011, **354**, 292–305.
71 Q. Yang, M. Gao, Z. Luo and S. Yang, *Chem. Eng. J.*, 2016, **285**, 27–38.
72 G. Xue, M. Gao, Z. Gu, Z. Luo and Z. Hu, *Chem. Eng. J.*, 2013, **218**, 223–231.
73 A. Abutaleb, M. Imran, N. Zouli, A. H. Khan, S. Hussain, M. A. Ali, O. Bakather, M. A. Gondal, N. A. Khan, H. Panchal and S. Zahmatkesh, *Chemosphere*, 2023, **316**, 137824.
74 C. V. Lazaratou, D. V. Vayenas and D. Papoulis, *Appl. Clay Sci.*, 2020, **185**, 105377.
75 A. Kausar, M. Iqbal, A. Javed, K. Aftab, Z. Nazli, H. N. Bhatti and S. Nouren, *J. Mol. Liq.*, 2018, **256**, 395–407.

76 M. A. Moreira, K. J. Ciuffi, V. Rives, M. A. Vicente, R. Trujillano, A. Gil, S. A. Korili and E. H. de Faria, *Appl. Clay Sci.*, 2017, **135**, 394–404.
77 T. Ngulube, J. R. Gumbo, V. Masindi and A. Maity, *J. Environ. Manage.*, 2017, **191**, 35–57.
78 H. Han, M. K. Rafiq, T. Zhou, R. Xu, O. Mašek and X. Li, *J. Hazard. Mater.*, 2019, **369**, 780–796.
79 N. Belhouchat, H. Zaghouane-Boudiaf and C. Viseras, *Appl. Clay Sci.*, 2017, **135**, 9–15.
80 H. Zaghouane-Boudiaf, M. Boutahala, S. Sahnoun, C. Tiar and F. Gomri, *Appl. Clay Sci.*, 2014, **90**, 81–87.
81 Q. Cui and B. Chen, *Appl. Clay Sci.*, 2023, **235**, 106869.
82 M. Arif, G. Liu, B. Yousaf, R. Ahmed, S. Irshad, A. Ashraf, M. Zia-ur-Rehman and M. S. Rashid, *J. Cleaner Prod.*, 2021, **310**, 127548.
83 M. M. Mian and G. Liu, *Chem. Eng. J.*, 2020, **392**, 123681.
84 K. S. D. Premarathna, A. Upamali, B. Sarkar and E. E. Kwon, *Chem. Eng. J.*, 2019, **372**, 536–550.
85 P. Pandey and V. K. Saini, *Environ. Chem. Lett.*, 2019, **17**, 721–727.
86 Z. Huang, P. Wu, B. Gong, Y. Dai, P. C. Chiang, X. Lai and G. Yu, *PLoS One*, 2016, **11**, e0159802.
87 M. Ding, S. Zuo and C. Qi, *Appl. Clay Sci.*, 2015, **115**, 9–16.
88 C. Liu, Z. Li, B. Li, H. Zhang and J. Han, *Appl. Clay Sci.*, 2023, **236**, 106887.
89 A. Bashir, S. Ahad, L. A. Malik, A. Qureashi, T. Manzoor, G. N. Dar and A. H. Pandith, *Ind. Eng. Chem. Res.*, 2020, **59**, 22353–22397.
90 M. Pica, *Molecules*, 2021, **26**, 2392.
91 R. Chakraborty, K. Bhattacharaya and P. Chattopadhyay, *Appl. Radiat. Isot.*, 2014, **85**, 34–38.
92 W. J. Mu, Q. H. Yu, R. Zhang, X. L. Li, R. Hu, Y. He, H. Y. Wei, Y. Jian and Y. C. Yang, *J. Mater. Chem. A*, 2017, **5**, 24388–24395.
93 A. Bashir, L. A. Malik, G. N. Dar and A. H. Pandith, in *Application of Ion Exchange Materials in the Environment*, ed. A. M. Inamuddin and A. Assiri, Springer, Cham, 2019, pp. 95–108.
94 W. J. Mu, S. Z. Du, Q. H. Yu, X. L. Li, H. Y. Wei, Y. C. Yang and S. M. Peng, *Chem. Eng. J.*, 2019, **361**, 538–546.
95 T. Takei, K. Iidzuka, A. Miura, S. Yanagida, N. Kumada, E. Magome, C. Moriyoshi and Y. Kuroiwa, *Langmuir*, 2016, **32**, 9993–9999.
96 Y. Cheng, X. D. Wang, S. Jaenicke and G. K. Chuah, *Inorg. Chem.*, 2018, **57**, 4370–4378.
97 S. Bevara, P. Giri, S. J. Patwe, S. N. Achary, R. K. Mishra, A. Kumar, A. K. Sinha, C. P. Kaushik and A. K. Tyagi, *J. Environ. Chem. Eng.*, 2018, **6**, 2248–2261.
98 Y. Cheng, S. S. Y. Chui, X. D. T. Wang, S. Jaenicke and G. K. Chuah, *Inorg. Chem.*, 2019, **58**, 13020–13029.
99 Y. Cheng, H. W. Zhang, J. A. Jaenicke, E. C. P. Tan and G. K. Chuah, *ACS Sustainable Chem. Eng.*, 2019, **7**, 895–904.
100 W. J. Mu, Q. H. Yu, J. Y. Gu, X. L. Li, Y. C. Yang, H. Y. Wei and S. M. Peng, *Sep. Purif. Technol.*, 2020, **240**, 116658.
101 A. M. Bakry, F. S. Awad, J. A. Bobb, A. A. Ibrahim and M. S. El-Shall, *RSC Adv.*, 2020, **10**, 37883–37897.
102 S. Fujimoto, T. Takei, S. Yanagida and N. Kumada, *J. Ceram. Soc. Jpn.*, 2019, **127**, 830–836.
103 R. Silbernagel, C. H. Martin and A. Clearfield, *Inorg. Chem.*, 2016, **55**, 1651–1656.
104 M. W. Terban, C. Shi, R. Silbemagel, A. Clearfield and S. J. L. Billinge, *Inorg. Chem.*, 2017, **56**, 8837–8846.
105 S. Pourbeyram, *Ind. Eng. Chem. Res.*, 2016, **55**, 5608–5617.
106 T. Ahamad, M. Naushad, B. M. Al-Maswari, J. Ahmed, Z. A. Alothman, S. M. Alshehri and A. A. Alqadami, *J. Ind. Eng. Chem.*, 2017, **53**, 268–275.
107 X. L. Zhang, J. L. Shen, S. Y. Pan, J. S. Qian and B. C. Pan, *Adv. Funct. Mater.*, 2020, **30**, 1909014.
108 D. D. Zhao, Y. Yu and J. P. Chen, *Water Res.*, 2016, **101**, 564–573.
109 J. H. Xu, R. Koivula, W. Z. Zhang, E. Wiikinkoski, S. Hietala and R. Harjula, *Hydrometallurgy*, 2018, **175**, 170–178.
110 Y. Ibrahim, E. Abdulkarem, V. Naddeo, F. Banat and S. W. Hasan, *Sci. Total Environ.*, 2019, **690**, 167–180.
111 R. Bhatt, V. Ageetha, S. B. Rathod and P. Padmaja, *Carbohydr. Polym.*, 2019, **208**, 441–450.
112 M. Thakur, D. Pathania, G. Sharma, M. Naushad, A. Bhatnagar and M. R. Khan, *J. Polym. Environ.*, 2018, **26**, 1415–1424.
113 Y. Zhu, T. Shimizu, T. Kitajima, K. Morisato, N. Moitra, N. Brun, T. Kiyomura, K. Kanamori, K. Takeda, H. Kurata, M. Tafu and K. Nakanishi, *New J. Chem.*, 2015, **39**, 2444–2450.
114 Q. R. Zhang, Y. X. Li, P. Phanlavong, Z. K. Wang, T. F. Jiao, H. Qiu and Q. M. Peng, *J. Cleaner Prod.*, 2017, **161**, 317–326.
115 S. Qing, H. Chen, L. J. Han, Z. B. Ye, L. T. Shi, Z. Shu, L. Chen, L. Xu and Q. Q. Xu, *ACS Omega*, 2020, **5**, 27873–27879.
116 Y. J. Zhou, J. J. Liu, M. Xiao, Y. Z. Meng and L. Y. Sun, *ACS Appl. Mater. Interfaces*, 2016, **8**, 5547–5555.
117 L. Ma, Q. Wang, S. M. Islam, Y. Liu, S. Ma and M. G. Kanatzidis, *J. Am. Chem. Soc.*, 2016, **138**(8), 2858–2866.
118 D. Cosano, D. Esquivel, F. J. Romero-Salguero, C. Jimenez-Sanchidrian and J. R. Ruiz, *Langmuir*, 2023, **39**, 5294–5305.
119 A. Haleem, A. Shafiq, S.-Q. Chen and M. Nazar, *Molecules*, 2023, **28**, 1081.
120 Y.-D. Dong, Y. Shi, Y.-L. He, S.-R. Yang, S.-Y. Yu, Z. Xiong, H. Zhang, G. Yao, C.-S. He and B. Lai, *Ind. Eng. Chem. Res.*, 2023, **62**, 10828–10848.
121 Z. Bi, R.-T. Guo, X. Hu, J. Wang, X. Chen and W.-G. Pan, *Nanoscale*, 2022, **14**(9), 3367–3386.
122 C. Zhao, L. Wang, L. Huang, N. M. Musyoka, T. Xue, J. Rabeah and Q. Wang, *J. Energy Chem.*, 2024, **90**, 435–452.
123 Z.-Y. Zhang, H. Tian, L. Bian, S.-Z. Liu, Y. Liu and Z.-L. Wang, *J. Energy Chem.*, 2023, **83**, 90–97.

124 X. Xu, J. Wang, A. Zhou, S. Dong, K. Shi, B. Li, J. Han and D. O'Hare, *Nat. Commun.*, 2021, **12**, 3069.
125 P. Zhang, J. Li, L. Lv, Y. Zhao and L. Qu, *ACS Nano*, 2017, **11**, 5087–5093.
126 J. Xue, S. Ma, Y. Zhou, Z. Zhang and M. He, *ACS Appl. Mater. Interfaces*, 2015, **7**(18), 9630–9637.
127 G. Mishra, B. Dash and S. Pandey, *Appl. Clay Sci.*, 2018, **153**, 172–186.
128 T. Hu, X. Mei, Y. Wang, X. Weng, R. Liang and M. Wei, *Sci. Bull.*, 2019, **64**, 1707–1727.
129 C. F. Gomes, J. H. Gomes and E. F. da Silva, *Environ. Geochem. Health*, 2020, **42**, 3507–3527.
130 P. Das, S. Manna, A. K. Behera, M. Shee, P. Basak and A. K. Sharma, *Environ. Res.*, 2022, **212**, 113534–123546.
131 A. Sharma, G. R. Kokil, Y. He, B. Lowe, A. Salam, T. A. Altalhi, Q. Ye and T. Kumeria, *Bioact. Mater.*, 2023, **24**, 535–550.
132 C. de Sousa Figueiredo Gomes, *Environ. Geochem. Health*, 2018, **40**, 1739–1765.
133 N. Khatoon, M. Q. Chu and C. H. Zhou, *J. Mater. Chem. B*, 2020, **8**, 7335–7351.
134 L. Jia, T. Zhou, J. Xu, Z. Xu, M. Zhang, Y. Wang, Z. Li and T. Zhu, *J. Mater. Sci.*, 2016, **5**, 1324–1332.
135 S. Murugesan and T. Scheibel, *J. Polym. Sci.*, 2021, **59**, 1610–1642.
136 H. Tomás, C. S. Alves and J. Rodrigues, *Nanomedicine*, 2018, **14**, 2407–2420.
137 Y. M. Lvov, Y. M. M. DeVilliers and R. F. Fakhrullin, *Expert Opin. Drug Delivery*, 2016, **13**, 977–986.
138 H. Y. Kim, J. H. Jae, H. Cheon, S. H. Lee, J. Y. Min, S.-Y. Back, J. G. Song, D. H. Kim, J.-J. Lim and H.-K. Han, *J. Nanobiotechnol.*, 2020, **18**, 17–31.
139 A. I. Voicu, S. A. Gârea, A. Ghebaur, C. L. Nistor, A. Sârbu, E. Vasile, R. Mitran and H. Iovu, *Microporous Mesoporous Mater.*, 2021, **328**, 111434.
140 F. García-Villén and C. Viseras, *Pharmaceutics*, 2020, **12**, 1142–1150.
141 C. Tipa, M. T. Cidade, T. Vieira, J. C. Silva, P. I. P. Soares and J. P. Borges, *Nanomaterials*, 2021, **11**(1), 25–47.
142 K. Dutta, K. Saha, P. Sarkar and D. Chattopadhyay, *Bull. Mater. Sci.*, 2020, **43**(1), 248–257.
143 A. Rapacz-Kmita, B. Szaraniec, M. Mikołajczyk, E. Stodolak-Zych, E. Dzierzkowska, M. Gajek and P. Dudek, *Acta Bioeng. Biomech.*, 2020, **22**(2), 83–93.
144 C. F. Memenfo, N. Tabary, J. A. Mbey, S. Degoutin, F. Cazaux, M. Bacquet, M. Maton, B. Martel and D. Njopwouo, *J. Mater. Sci. Chem. Eng.*, 2021, **9**, 21–40.
145 H.-J. Huang, S.-Y. Huang, T.-H. Wang, T.-Y. Lin, N.-C. Huang, O. Shih, U.-S. Jeng, C.-Y. Chu and W.-H. Chiang, *Carbohydr. Polym.*, 2023, **302**, 120390.
146 J. J. Zhang, F. Zhou, Z. He, Y. Pan, S. Zhou, C. Yan, L. Luo and Y. Gao, *ACS Appl. Mater. Interfaces*, 2022, **14**(27), 30533–30545.
147 D. Peixoto, I. Pereira, M. Pereira-Silva, F. Veiga, M. R. Hamblin, Y. Lvov, M. Liu and A. C. Paiva-Santos, *Coord. Chem. Rev.*, 2021, **440**, 213956.
148 M. Massaro, C. G. Colletti, G. Lazzara and S. Riela, *J. Funct. Biomater.*, 2018, **9**, 58–70.
149 D. Sawicka, L. Zapor, L. Chojnacka-Puchta and K. Miranowicz-Dzierzawska, *Toxicol. Res.*, 2021, **37**, 301–331.
150 G. Biddeci, G. Spinelli, P. Colomba and F. Di Blasi, *Int. J. Mol. Sci.*, 2023, **24**(5), 4801–4822.
151 Q. Pan, N. Li, Y. Hong, H. Tang, Z. Zheng, S. Weng, Y. Zheng and L. Huang, *RSC Adv.*, 2017, **7**(34), 21352–21359.
152 M. Barman, S. Mahmood, R. Augustine, A. Hasan, S. Thomas and K. Ghosal, *Int. J. Biol. Macromol.*, 2020, **162**, 1849–1861.
153 R. Shi, Y. Niu, M. Gong, J. Ye, W. Tian and L. Zhang, *Mater. Sci. Eng., C*, 2018, **87**, 128–138.
154 C. Zagni, A. A. Scamporrino, P. M. Riccobene, G. Floresta, V. Patamia, A. Rescifina and S. C. Carroccio, *Nanomaterials*, 2023, **13**, 741.
155 R. Arshad, M. S. Arshad, A. Rahdar, D. Hassan, R. Behzadmehr, S. Ghotekar, D. I. Medina and S. Pandey, *J. Drug Delivery Sci. Technol.*, 2023, **83**, 104432–104444.
156 K. Li, Y. Zhang, M. Chen, Y. Hu, W. Jiang, L. Zhou, S. Li, M. Xu, Q. Zhao and R. Wan, *Int. J. Nanomed.*, 2018, **13**, 19–30.
157 M. Perveen, S. Nazir, A. W. Arshad, M. I. Khan, M. Shamim, K. Ayub, M. A. Khan and J. Iqbal, *Biophys. Chem.*, 2020, **267**, 106461–106473.
158 E. Naumenko and R. Fakhrullin, *Biotechnol. J.*, 2019, e1900055.
159 E. Gkouma, E. Gianni, K. Avgoustaki and D. Papoulis, *Appl. Clay Sci.*, 2021, **214**, 106291.
160 L. W. Wong, C. B. S. Goh, P. Pasbakhsh and J. B. L. Tan, *J. Sci.-Adv. Mater. Dev.*, 2022, **7**, 100431–100445.
161 F. Kazemi-Aghdam, V. Jahed, M. Dehghan-Niri, F. Ganji and E. Vasheghani-Farahani, *Carbohydr. Polym.*, 2021, **269**, 118311–118320.
162 M. A. Bonifacio, A. Cochis, S. Cometa, A. Scalzone, P. Gentile, G. Procino, S. Milano, A. C. Scalia, L. Rimondini and E. De Giglio, *Mater. Sci. Eng., C*, 2020, **108**, 110444.
163 B. M. Dharmaraj, R. Subramani, G. Dhanaraj and K. Louis, *Compos., Part C: Open Access*, 2020, **3**, 10007–10019.
164 S. Mehnath and M. Jeyaraj, *Mater. Chem. Phys.*, 2023, **295**, 127061–127074.
165 J. Ji, C. Wang, Z. Xiong, Y. Pang and W. Sun, *Mater. Today Adv.*, 2022, **15**, 100259–100271.
166 S. Marchesi, F. Carniato, C. Bisio, L. Tei, M. Botta and L. Marchese, *Dalton Trans.*, 2018, **47**, 7896–7904.
167 S. Marchesi, D. Lalli, F. Carniato, C. Bisio, L. Tei, L. Marchese and M. Botta, *Dalton Trans.*, 2020, **49**, 6566–6571.
168 T. Zhou, L. Jia, Y. F. Luo, J. Xu, R. H. Chen, Z. J. Ge, T. L. Ma, H. Chen and T. F. Zhu, *J. Nanomed.*, 2016, **11**, 4765–4776.

169 G. Basina, G. Diamantopoulos, E. Devlin, V. Psycharis, S. M. Alhassan, M. Pissas, G. Hadjipanayis, A. Tomou, A. Bouras, C. Hadjipanayis and V. Tzitzios, *J. Mater. Chem. B*, 2022, **10**, 4935–4945.
170 M. V. Ramos-Garcés, J. González-Villegas, A. López-Cubero and J. L. Colón, *Acc. Mater. Res.*, 2021, **2**, 793–803.
171 A. Donnadio, G. Paul, M. Barbalinardo, V. Ambrogi, G. Pettinacci, T. Posati, C. Bisio, R. Vivani and M. Nocchetti, *Nanomaterials*, 2023, **13**, 742.
172 M. Pica, A. Donnadio and M. Casciola, *Coord. Chem. Rev.*, 2018, **374**, 218–235.
173 M. L. González, M. Ortíz, C. Hernández, J. Cabán, A. Rodríguez, J. L. Colón and A. Báez, *J. Nanosci. Nanotechnol.*, 2016, **16**, 117–129.
174 J. González-Villegas, Y. Kan, V. I. Bakhmutov, A. García-Vargas, M. Martínez, A. Clearfield and J. L. Colón, *Inorg. Chim. Acta*, 2017, **468**, 270–279.
175 H. Kalita, B. N. P. Kumar, S. Konar, S. Tantubay, M. K. Mahto, M. Mandal and A. Pathak, *Mater. Sci. Eng., C*, 2016, **60**, 84–91.
176 H. Kalita, S. Rajput, B. N. P. Kumar, M. Mandal and A. Pathak, *RSC Adv.*, 2016, **6**, 21285.
177 S. Yu, X. Gao, H. Baigude, X. Hai, R. Zhang, X. Gao, B. Shen, Z. Li, Z. Tan and H. Su, *ACS Appl. Mater. Interfaces*, 2015, **7**, 5089–5096.
178 R. Hosseinzadeh and K. Khorsandi, *Sci. Rep.*, 2019, **9**, 14899.
179 A. Donnadio, V. Ambrogi, D. Pietrella, M. Pica, G. Sorrentino and M. Casciola, *RSC Adv.*, 2016, **6**, 46249–46257.
180 I. García, C. Trobajo, Z. Amghouz and A. Adawy, *Materials*, 2021, **14**, 1481.
181 M. Pica, N. Messere, T. Felicetti, S. Sabatini, D. Pietrella and M. Nocchetti, *Materials*, 2021, **14**, 670.
182 H. Ueoka, O. Shimomura, M. Pica, A. Donnadio and R. Nomura, *Colloids Interface Sci. Commun.*, 2019, **28**, 29–33.
183 M. Bastianini, M. Sisani, A. Petracci, I. Di Guida, C. Faffa and F. Cardellini, *Mater. Adv.*, 2021, **2**, 1313–1319.
184 M. Camara-Torres, S. Duarte, R. Sinha, A. Egizabal, N. Alvarez, M. Bastianini, M. Sisani, P. Scopece, M. Scatto, A. Bonetto, A. Marcomini, A. Sanchez, A. Patelli, C. Mota and L. Moroni, *Bioact. Mater.*, 2021, **6**, 1073–1082.
185 H. Du, D. Zhang, F. Peng, K. W. K. Yeung and X. Liu, *Prog. Mater. Sci.*, 2024, **142**, 101220.
186 S. Kumari, V. Sharma, S. Soni, A. Sharma, A. Thakur, S. Kumar, K. Dhama, A. K. Sharma and S. K. Bhatia, *Environ. Res.*, 2023, **238**, 117171.
187 Y. Bian, X. Cai, Z. Lv, Y. Xu, H. Wang, C. Tan, R. Liang and X. Weng, *Adv. Sci.*, 2023, **10**, 2301806.
188 S. Karimi, H. Rasuli and R. Mohammadi, *Int. J. Biol. Macromol.*, 2023, **234**, 123538.
189 V. R. L. Constantino, M. P. Figueiredo, V. R. Magri, D. Eulalio, V. R. R. Cunha, A. C. S. Alcantara and G. F. Perotti, *Pharmaceutics*, 2023, **15**, 413.
190 C. Nomicisio, M. Ruggeri, E. Bianchi, B. Vigani, C. Valentino, C. Aguzzi, C. Viseras, S. Rossi and G. Sandri, *Pharmaceutics*, 2023, **15**, 1368.
191 Q. Li, X. Wu, S. Mu, C. He, X. Ren, X. Luo, M. Adeli, X. Han, L. Ma and C. Cheng, *Adv. Sci.*, 2023, **10**, 2207759.
192 J.-H. Yang, J.-H. Lee, H.-J. Ryu, A. A. Elzatahry, Z. A. Alothman and J.-H. Choy, *Appl. Clay Sci.*, 2016, **130**, 20–32.
193 G. Choi, S. Eom, A. Vinu and J.-H. Choy, *Chem. Rec.*, 2018, **18**, 1033–1053.
194 S. S. Shafiei, M. Shavandi, G. Ahangari and F. Shokrolahi, *Appl. Clay Sci.*, 2016, **127**, 52–63.
195 F. Perreault, A. Fonseca de Faria, S. Nejati and M. Elimelech, *ACS Nano*, 2015, **9**(7), 7226–7236.
196 G. Reina, J.-M. Gonzalez-Dominguez, A. Criado, E. Vazquez, A. Bianco and M. Prato, *Chem. Soc. Rev.*, 2017, **46**(15), 4400–4416.
197 P. Das, S. Manna, A. K. Behera, M. Shee, P. Basak and A. K. Sharma, *Environ. Res.*, 2022, **212**, 113534–123546.
198 R. Mukhopadhyay, D. Bhaduri, B. Sarkar, R. Rusmin, D. Hou, R. Khanam, S. Sarkar, J. K. Biswas, M. Vithanage, A. Bhatnagar and Y. S. Ok, *J. Hazard. Mater.*, 2020, **383**, 121125.
199 X. Fu, J. Lin, Z. Liang, R. Yao, W. Wu, Z. Fang, W. Zou, Z. Wu, H. Ning and J. Peng, *Surf. Interfaces*, 2023, **37**, 102747.
200 S. Gungordu Er, M. Edirisinghe and T. A. Tabish, *Adv. Healthcare Mater.*, 2023, **12**, 2201523.
201 X. You, Q. Zhang, J. Yang and S. Dong, *Composites, Part A*, 2023, **167**, 107420.
202 S. Ren, M. Cui, C. Liu and L. Wang, *Corros. Sci.*, 2023, **212**, 110939.
203 *Polymer Nanocomposites Containing Graphene: Preparation, Properties, and Applications*, ed. M. Rahaman, L. Nayak, I. A. Hussein and N. C. Das, Woodhead Publishing, 2022.
204 C. Cheng, W. Song, Q. Zhao and H. Zhang, *Nanotechnol. Rev.*, 2020, **9**, 323–344.
205 H. W. Huang, X. X. Sheng, Y. Q. Tian, L. Zhang, Y. Chen and X. Y. Zhang, *Ind. Eng. Chem. Res.*, 2020, **59**(35), 15424–15446.
206 H. Huang, M. Li, Y. Tian, Y. Xie, X. Sheng, X. Jiang and X. Zhang, *Prog. Org. Coat.*, 2020, **138**, 105390.
207 T. C. Huang, G. H. Lai, C. E. Li, M. W. Tsai, P. Y. Wang, Y. H. Chung and M. H. Lin, *RSC Adv.*, 2017, **7**(36), 22540–22540.
208 S. L. Li, C. X. Zhao, H. L. Gou, Y. T. Li, X. J. He and L. Zhao, *Int. J. Electrochem. Sci.*, 2018, **13**(3), 2661–2675.
209 C. X. Zhao, P. Li, D. He, Y. T. Li, F. Lei and H. J. Sue, *RSC Adv.*, 2016, **6**, 73485–73495.
210 Y. F. Xiao, J. Y. Xu, S. W. Huang and H. M. Deng, *Int. J. Polym. Sci.*, 2017, 6034741.
211 K. Q. Li, H. M. Lei, X. R. Zeng, H. Q. Li, X. J. Lai and S. Y. Chai, *RSC Adv.*, 2017, **7**, 49290–49298.
212 L. F. Xu, C. H. Lei, R. J. Xu, X. Q. Zhang and F. Zhang, *Polym. Degrad. Stab.*, 2016, **133**, 378–388.
213 L. F. Xu, C. H. Lei, R. J. Xu, X. Q. Zhang and F. Zhang, *RSC Adv.*, 2016, **6**, 77545–77552.

214 E. N. Kalali, S. De Juan, X. Wang, S. Nie, R. Wang and D.-Y. Wang, *J. Therm. Anal.*, 2015, **121**, 619–626.
215 D. D. Yang, Y. Hu, H. T. Li, L. Song, H. P. Xu and B. Li, *J. Therm. Anal.*, 2015, **119**, 619–624.
216 D. Wang, H. Y. Peng, B. Yu, K. Q. Zhou, H. F. Pan, L. P. Zhang, M. Li, M. Liu, A. L. Tian and S. H. Fu, *Chem. Eng. J.*, 2020, **389**, 124449.
217 B. Ghanbarzadeh, S. A. Oleyaei and H. Almasi, *Crit. Rev. Food Sci. Nutr.*, 2015, **55**, 1699–1723.
218 D. Han, Y. Luo, Q. Ju, X. Xiao, M. Xiao, N. Xiao, S. Chen, X. Peng, S. Wang and Y. Meng, *Polymers*, 2018, **10**, 1082.
219 H. Oosthuizen, L. Jones, S. Naseem, F. J. W. J. Labuschagne and A. Leuteritz, *J. Polym. Sci.*, 2023, **61**, 1749–1777.
220 S. Kumari, S. Soni, Aj. Sharma, S. Kumar, V. Sharma, V. S. Jaswal, S. K. Bhatia and A. K. Sharma, *Appl. Clay Sci.*, 2024, **247**, 107216.
221 Y. Guo, F. Leroux, W. Tian, D. Li, P. Tang and Y. Feng, *Appl. Clay Sci.*, 2021, **211**, 106198.
222 A. A. Marek, V. Verney, G. Totaro, L. Sisti, A. Celli, N. Bozzi Cionci, D. Di Gioia, L. Massacrier and F. Leroux, *Appl. Clay Sci.*, 2020, **188**, 105502.
223 S. Coiai, F. Cicogna, S. Pinna, R. Spiniello, M. Onor, W. Oberhauser, M.-B. Coltelli and E. Passaglia, *Appl. Clay Sci.*, 2021, **214**, 106276.
224 Q. Zhang, Y. Guo, F. Leroux, P. Tang, D. Li, L. Wang and Y. Feng, *New J. Chem.*, 2020, **44**(24), 10119–10126.
225 J. Zhang, Q. Ke, J. Bai and M. Yang, *Polym. Degrad. Stab.*, 2023, **218**, 110550.
226 L. Han, J. Geng, Z. Wang and J. Hua, *Polym. Adv. Technol.*, 2022, **33**, 3619–3627.
227 Y. Feng, Y. Jiang, Q. Huang, S. Chen, F. Zhang, P. Tang and D. Li, *Ind. Eng. Chem. Res.*, 2014, **53**(6), 2287–2292.
228 Q. Zhang, Y. Guo, A. A. Marek, V. Verney, F. Leroux, P. Tang, D. Li and Y. Feng, *Inorg. Chem. Front.*, 2019, **6**, 2539–2549.
229 Q. Zhang, Q. Gu, F. Leroux, P. Tang, D. Li and Y. Feng, *Beilstein J. Nanotechnol.*, 2018, **9**, 2980–2988.
230 N. K. Kumbhar, M. D. Joshi, V. Kumar and S. S. Hosmani, *Adv. Eng. Mater.*, 2023, **25**, 2201680.
231 A. Chaouiki, M. Chafiq, T. Suhartono and Y. G. Ko, *Chem. Eng. J.*, 2023, **470**, 144355.
232 F. G. Nunes Filho, E. C. Silva Filho, J. A. Osajima, A. P. de Melo Alves and M. G. Fonseca, *Appl. Clay Sci.*, 2023, **239**, 106952.
233 Z. Chen, G.-F. Han, A. Mahmood, J. Hou, W. Wei, H. K. Shon, G. Wang, T. D. Waite, J.-B. Baek and B.-J. Ni, *Prog. Mater. Sci.*, 2024, **145**, 101299.
234 D. Evis, M. M. Ba-Abbad, A. Benamor and M. H. El-naas, *Appl. Clay Sci.*, 2022, **229**, 106686.
235 C. Zhu, J. Jiang, Y. Jia, Z. P. Xu and L. Zhang, *Acc. Mater. Res.*, 2023, **4**, 758–771.
236 H. Desai, A. Kannan and G. S. K. Reddy, *Microporous Mesoporous Mater.*, 2023, **352**, 112488.